Molecular and functional heterogeneity of cancer associated fibroblasts in high-grade serous ovarian cancer

Ali Hussain[1], Veronique Voisin[2], Stephanie Poon[1], Julia Dmytryshyn[3], Cory Richman[1], Jalna Meens[3], Victor W Ho[3], Kwan Ho Tang[4], Joshua Paterson[3], Blaise Clarke[5], Marcus Q Bernardini[6], Gary D Bader[2, 7], Benjamin G Neel[1, 3 4], Laurie E Ailles[1,3,8,*].

Affiliations:

[1]Department of Medical Biophysics, University of Toronto, Toronto, ON, Canada

[2]The Donnelly Centre, University of Toronto, Toronto, ON, Canada

[3]Princess Margaret Cancer Centre, University Health Network, Toronto, ON, Canada

[4] Laura and Isaac Perlmutter Cancer Center, New York Langone Health, New York, NY.

[5]Department of Laboratory Medicine and Pathobiology, University of Toronto, Toronto, ON, Canada; Department of Pathology, University Health Network, Toronto, ON, Canada

[6]Division of Gynaecologic Oncology, University Health Network, Toronto, Ontario, Canada

[7]Department of Molecular Genetics, University of Toronto, Toronto, ON, Canada.

[8]Lead contact

*Correspondence: lailles@uhnresearch.ca.

SUMMARY

Recent studies indicate that cancer-associated fibroblasts (CAFs) are phenotypically and functionally heterogeneous. However, little is known about CAF subtypes and the roles they play in cancer progression. Here we identify and characterize two CAF subtypes that coexist within high grade serous ovarian cancers: Fibroblast activation protein (FAP)-high (FH) CAFs resemble the classical myofibroblast-type CAF, whereas FAP-low (FL) CAFs possesses a preadipocyte-like molecular signature. Patients with predominantly FH CAFs have significantly worse outcomes than patients with predominantly FL CAFs. FH CAFs contract collagen gels and aggressively promote proliferation, invasion and therapy resistance of cancer cells, whereas FL CAFs do not. Overexpression of the FL-specific transcription factor TCF21 in FH CAFs decreases their ability to promote gel contraction, invasion, and *in vivo* tumor growth. Understanding CAF subtypes in more detail could lead to better patient stratification and novel therapeutic strategies.

Keywords: high-grade serous ovarian cancer; cancer-associated fibroblasts; tumor microenvironment; molecular heterogeneity; cancer cell invasion, chemotherapy resistance; TCF21

INTRODUCTION

High grade serous ovarian cancer (HGSOC) is the most common histological subtype of ovarian cancer and is typically diagnosed at an advanced stage (Ledermann et al., 2013). Optimal surgical debulking and platinum/taxane-based chemotherapy significantly increase the survival of HGSOC patients, but the vast majority relapse within 5 years of diagnosis and die of their disease (Ledermann et al., 2013). Due to early dissemination and implantation of cancer cells within the peritoneal cavity, HGSOC patients typically present at late stage with widespread abdominal disease, and nearly invariably develop chemotherapy resistance. In spite of recent advances with targeted therapies such as PARP inhibitors (Moore et al., 2018), bevacizumab (Monk et al., 2016), and immune checkpoint blockade (Hamanishi et al., 2015), these approaches do not currently benefit all patients and mortality rates remain high. The development of more effective treatments for HGSOC patients thus remains a necessary and important goal.

Cancer-associated fibroblasts (CAFs) are a key component of the tumor microenvironment and have several differences relative to their normal counterparts, including increased proliferation, extracellular matrix production, and expression of cytokines and growth factors (Junttila and de Sauvage, 2013). In many cancers, including HGSOC, CAFs have important effects on tumor behavior, including defining the rate and extent of cancer progression through inhibition of cancer cell apoptosis, induction of cancer cell proliferation, promotion of cancer cell migration and invasion and mediation of chemotherapy resistance (Kalluri, 2016; Mhawech-Fauceglia et al., 2015; Ryner et al., 2015; Thibault et al., 2014; Yeung et al., 2016). More recently CAFs have also been shown to mediate immune-suppression (Fearon, 2014; Kraman et al., 2010; Yang et al., 2016), adding another layer of complexity to their pro-tumorigenic role. A variety of markers have been used to identify CAFs, including α-smooth muscle actin (SMA), platelet-derived growth factor receptors (PDGFRs) and fibroblast activation protein (FAP), and most studies have focused on CAFs that express these markers. However, more recent studies have shown that CAFs are heterogeneous, and CAF subsets with distinct phenotypes and functions have begun to be identified in various malignancies (Costa et al., 2018; Givel et al., 2018; Ohlund et al., 2017; Su et al., 2018; Sugimoto et al., 2006).

Here we describe the identification of two distinct CAF subtypes in primary HGSOC specimens. We identify subtype-specific gene signatures that are prognostic in HGSOC patients,

and use *in vitro* and *in vivo* assays to reveal functional differences between the two subtypes. We also show that CAF identity is regulated, at least in part, by transcription factor TCF21.

RESULTS

Isolation and transcriptional profiling of CAFs from primary HGSOC tumor samples

Purification of viable CAFs directly from primary tumors using fluorescence activated cell sorting (FACS) requires a robust cell surface marker. PDGFR-β and FAP are commonly used CAF markers but we found these to be either dimly or inconsistently expressed in single cell suspensions from primary HGSOC samples, in line with other studies showing that expression of established CAF markers is heterogeneous and non-overlapping (Orimo and Weinberg, 2007; Sugimoto et al., 2006). We therefore used high-throughput flow cytometry with a panel of 363 antibodies targeting cell surface proteins (Gedye et al., 2014) to analyze cultured CAF lines derived from four HGSOC patients and single cell suspensions from five primary HGSOC samples. The latter were co-stained for CD45 and CD31 to allow exclusion of contaminating immune and endothelial cells, respectively. From this screen we identified several proteins that were uniformly highly expressed on the cultured CAFs, but only stained a minority of the CD45-/CD31- cells from primary HGSOC samples, which would be expected to contain a mixture of cancer cells and CAFs (**Figure S1**). The greatest difference was seen for CD49e (ITGA5), which was selected for follow-up. Immunofluorescence studies of HGSOC sections confirmed that CD49e antibody selectively stained the tumor stromal compartment, while pan-CK antibody, as expected, stained tumor cells (**Figure 1A**). Co-staining with an anti-EpCAM antibody (an epithelial cell marker) enabled clear distinction and isolation of CAFs from HGSOC samples as the CD45-CD31-EpCAM-CD49e+ fraction, which varied in frequency between patients (**Figure 1B**). The identity of isolated CD45-CD31-EpCAM+CD49e- (referred to as EpCAM+) and CD45-CD31-EpCAM-CD49e+ (referred to as CD49e+) fractions as cancer cells and CAFs, respectively, was further validated by generating cytospins of the purified populations and staining them for pan-CK, Vimentin and p53. The CD49e+ fraction was positive for Vimentin and negative for pan-CK, as would be expected for a fibroblast population (**Figure 1C**). In addition, in patients for whom the EpCAM+ fraction showed strong nuclear P53 staining, indicative of mutant P53 (Kobel et al., 2016), the CD49e+ fraction was negative for P53 staining, demonstrating that CD49e+ cells

do not bear the cancer-associated mutation and ruling out the possibility that they are cancer cells that underwent an epithelial-to-mesenchymal transition (EMT; **Figure 1D**).

To interrogate the transcriptional profiles of cells isolated directly from primary tumor specimens, FACS was used to isolate the CD49e+ fraction and the EpCAM+ fraction from 12 primary HGSOC samples (**Figure S2A**). The latter was further fractionated into EpCAM+CD133+ and EpCAM+CD133- fractions, as we had previously shown that CD133 was a marker of tumor-initiating cells in the majority of primary HGSOC solid tumors (Stewart et al., 2011). RNA was extracted and analyzed using Illumina HT-12v4 microarrays. Upon unsupervised analysis, CD133+ and CD133- subsets had very similar transcriptional profiles and clustered together, whereas the CD49e+ population formed a distinct cluster (**Figure 1E**). The CD49e+ fraction expressed known CAF-associated genes, including *ACTA2, FAP, VIM, POSTN, SPARC*, and multiple collagen genes, among others (**Table S2A**). Gene set enrichment analysis (GSEA) was carried out on differentially expressed genes between CD49e+ cells and EpCAM+ cells using the MsigDB Reactome database. EpCAM+ cells were enriched for genes related to cell proliferation, metabolism and epithelial identity (e.g., tight junction interactions, cell-cell junction organization), whereas the CD49e+ subset was enriched for gene sets involved in extracellular matrix organization, myogenesis and known mesenchymal signaling pathways, such as PDGF, FGF and RHO GTPase signaling (Kuzet and Gaggioli, 2016; Zhou et al., 2013). These results further confirm the identity of our purified CD49e+ population as fibroblasts (**Figure 1F, Table S2B)**.

The CD49e+ fraction separates into 2 clusters

Unsupervised hierarchical clustering of the microarray data indicated that the CD49e+ CAF population segregated into two sub-clusters (**Figure 1E, Figure S2B**), suggesting that CAFs derived from HGSOC patients are heterogeneous. One cluster expressed classical CAF-related genes, such as *FAP*, *TGFβ*, *COL11A1*, *SULF1* and inflammatory cytokines (e.g., *IL-6, CXCL12*), among others, whereas the other exhibited a distinct gene expression profile that included low expression of the classical CAF marker *FAP* (**Figure 2A**, **Table S3A**). We therefore refer to these two groups of patients as "FAP-High" (FH) and "FAP-Low" (FL). Several of the FH (*FAP*, *COL11A1, SULF1*)- and FL (*DLK1*, *TCF21, COLEC11)*-specific genes were validated by reverse-transcription and quantitative polymerase chain reaction (qRT-PCR) on RNA isolated from the CD49e+ fraction of six patients included in the microarray analysis, three from the FH group and

three from the FL group (**Figure 2B**). To test whether the two CAF subtypes were a general feature of ovarian cancer stroma, we analyzed the gene expression data set generated by Leung and colleagues (Leung et al., 2014) who used laser capture microdissection to isolate stromal and epithelial components from 31 HGSOC specimens and 8 normal ovary specimens. We interrogated the expression of the top 500 differentially expressed genes between our FH and FL patients in the stromal samples from this cohort and again found two major clusters (**Figure 2A**). This result verified the ability of our FH *vs* FL gene list to segregate HGSOC patients into two subtypes based on expression of these genes in their stroma. Importantly, the transcriptional profile of normal ovarian stroma was distinct from the FL cancer stroma, indicating that FL CAFs represent a distinct phenotype of stromal cells within HGSOC, and not normal fibroblasts (**Figure S2C-D and Table S3B**).

FH and FL fibroblasts co-exist in the majority of patients.

To further interrogate the FH and FL status of patients classified into these groups by microarray analysis, we performed immunofluorescence (IF) staining for FAP, TCF21 (a highly-expressed FL gene) and pan-CK on serial sections from five tumors categorized as FH (n=3) or FL (n=2) by microarray. The slides were scanned to generate high resolution digital images of the entire section, and the FAP-positive or TCF21-positive stained areas within the Pan-CK negative, stromal regions were quantified using HALO image analysis software (**Figure 2C and Figure S3**). This analysis showed that FH patients indeed had more FAP-expressing cells in their tumor stroma than FL patients, whereas TCF21-expressing cells were more abundant in FL patients. However, we also noticed that within tumor samples, FAP-positive and TCF21-positive cells could both be observed, and regions with predominantly one type of CAF or the other could be identified (**Figure 2D**). Nevertheless, quantification by HALO indicated an anti-correlation between FAP and TCF21 expression (**Figure 2E**). Thus FH and FL CAFs are two distinct subtypes that co-exist within HGSOC tumors at varying ratios.

To more accurately quantify FH and FL CAFs within patient specimens, we performed flow cytometry on 66 HGSOC samples, with the addition of a FAP antibody to the previous combination of CD45, CD31, EpCAM and CD49e, allowing us to quantify FAP expression within the CD49e+ fraction. The FH subset ranged from 0.6% to 98% within the CD49e+ population (**Figure 2F**). Of the 5 patient samples that were also stained by IF, the flow cytometry and

immunofluorescence assays showed a strong positive correlation in the proportion of cells expressing FAP (r=0.969).

Transcriptional profiling of purified FH and FL cells

Our initial microarray analysis was performed on the bulk CD49e+ fraction, which contained mixtures of FH and FL CAFs at varying ratios, suggesting that the observed clustering of patients into FH and FL groups reflected the predominant population, but these populations were not pure. We therefore carried out RNA-Seq analysis on FH and FL CAFs purified by FACS. For some of these samples, the CD49e+ fraction was predominantly FH or FL, making isolation of both fractions in sufficient numbers difficult; however, for three patients (72143, 70535 and 71423), we successfully generated high-quality RNA-Seq data on both fractions. Principal component analysis of the five FH populations and four FL populations showed that regardless of whether the samples were derived from a FH patient or a FL patient, the samples clustered based on FAP status (**Figure 3A**). Gene set enrichment analysis (GSEA) comparing the genes differentially expressed in isolated FH and FL cells showed a very high concordance with the previously obtained microarray-derived gene lists (**Figure 3B**). In addition, *FAP*, *COL11A1* and *SULF1* were highly expressed in the FH subset, and *TCF21*, *COLEC11* and *DLK1* were highly expressed in the FL subset (**Figure 3C**). These results confirm that HGSOC samples contain mixtures of FH and FL CAFs at varying ratios, and that the clustering of patients based on bulk fibroblast profiling was driven by whichever population was dominant in those tumors.

There were 800 differentially expressed genes between FH and FL CAFs at a false discovery rate (FDR) value of ≤0.05 **(Table S4A).** GSEA of the differentially expressed genes between FH and FL cells (**Figure 3D**) showed that FH cells express genes involved in ECM reorganization, cell migration and chemotaxis, immune regulation (including neutrophil activation, regulation of defense response and antigen processing), and regulation of angiogenesis, and thus resemble the classical phenotype that is commonly associated with CAFs in the literature (Fearon, 2014; Kalluri and Zeisberg, 2006; Kuzet and Gaggioli, 2016)**.** By contrast, the most dominant gene sets expressed in FL CAFs include glucose/insulin homeostasis, cardiac muscle contraction and ion transport, translation and protein localization, and lipid metabolism**.** FL CAFs thus represent a previously unrecognized CAF subtype with a distinct gene expression profile from FH CAFs.

FH and FL patients can be identified in The Cancer Genome Atlas (TCGA) HGSOC dataset and have distinct clinical outcomes.

Gene expression profiling of 489 HGSOC samples by TCGA previously led to identification of four molecular subtypes: mesenchymal, proliferative, differentiated, immunoreactive (Cancer Genome Atlas Research, 2011). Refined signatures for these subtypes were subsequently generated, and the mesenchymal subtype was found to be associated with worse outcome (Verhaak et al., 2013). We generated a gene signature based on FH and FL CAF genes by filtering for genes that were both differentially expressed in purified FH *vs* FL cells, and differentially expressed in CAFs compared to EpCAM+ cells in our original microarray data set. This analysis resulted in a list of 165 FH-specific genes and 78 FL-specific genes (Figure S4A, Table S5). We then interrogated this signature against TCGA RNA-Seq data (n = 374 patients) and found that FH and FL transcripts were detectable in a large number of patients, with distinct FH and FL clusters present (Figure 4A). A scoring system was established to classify patients (Figure S4B). When a patient expressed 75% of the FH genes at a level higher than the population mean, the patient was classified FH (shown in black in Figure 4A). A second, less stringent threshold classified patients as FH if they expressed 50% of the FH genes above the mean (shown in grey in Figure 4A). The same rule was applied to classify the FL patients (shown in red and pink, respectively in Figure 4A). The majority of the FH patients overlapped with the TCGA mesenchymal subtype, whereas the FL patients were distributed amongst the mesenchymal, proliferative and differentiated subtypes (Figure 4A, Figure S4C). GSEA shows that the FH genes were highly enriched in the mesenchymal signature (Verhaak et al., 2013) whereas the FL genes were not (Figure 4B), suggesting that that the mesenchymal subtype is largely driven by the presence of FH fibroblasts.

Using the ABSOLUTE algorithm, which uses somatic copy number data to estimate the cellularity of tumor samples (Carter et al., 2012), it was shown previously that the mesenchymal subtype in the TCGA HGSOC study had the lowest tumor purity (Zhang et al., 2015). Using the same algorithm, FH and FL TCGA patients both had lower tumor purities than the remaining "other" patients that did not fall into either category (Figure 4C and Figure S4D). Histopathology data for the TCGA samples also indicates that tumor samples in the "other" category had a lower stromal content than both the FH and FL categories (Figure S4E). Taken together, these findings suggest that the unclassified samples could not be classified as FH or FL due to low stromal content within the tumor specimen analyzed.

ESTIMATE is another algorithm designed to estimate the quantity of infiltrating fibroblasts and immune cells using gene expression data on tumor tissues (Yoshihara et al., 2013). While the ESTIMATE algorithm generated a high "stromal" score for the FH samples, it failed to identify higher stromal content in tumor samples falling into the FL category (Figure 4C and Figure S4D). Deeper analysis of this discrepancy showed that the list of 141 genes used to define "stroma" in the ESTIMATE algorithm is enriched for FH genes (21-gene overlap), but not for FL genes (2-gene overlap). As a result, patients with a high fraction of FL CAFs were not identified as having higher stromal content using this algorithm.

To determine if the CAF subtype has an impact on survival, we performed a Kaplan-Meier analysis of the TCGA patients that were classified as FH or FL (using the more stringent cut-off of 75%). FH patients had significantly shorter progression-free and overall survival than FL patients; the median overall survival of FL patients was 2 years longer than that of FH patients (**Figure 4D**). To validate this finding, we compared the %FAP+ CAFs from patients that were analyzed by flow cytometry in Figure 2F to progression-free survival (determined by CA125 levels) for 46 of the patients for which these data were available. We defined FH patients as those with a %FAP+ CAFs above the median, and FL patients as those with a %FAP+ CAFs below the median. Current standard of care uses CA125 as a biomarker for relapse following initial treatment. We found that CA125 levels rose above the accepted threshold (35U/ml) significantly more rapidly in FH patients compared to FL patients. The median recurrence time for FH patients was 1.7 years compared to 3.4 years for FL patients (**Figure 4E).**

FL cells require different culture conditions than FH cells

Most studies of CAFs utilize cultures established by plating tumor cell suspensions onto tissue culture plastic in the presence of 10% fetal bovine serum (FBS). In these conditions, CAFs rapidly adhere and proliferate, allowing for their selection and outgrowth. Our identification of CD49e as a CAF marker was facilitated by analysis of such patient-derived cultured CAF lines. Analysis of several of our cultured CAF lines indicated that they are FH by flow cytometry and express FH but not FL genes (data not shown). When we placed FH and FL cells purified by FACS directly from patient samples into standard 10% FBS conditions, we found that FH cells had a significantly higher growth rate than FL cells, and that FL cells in these conditions did not reach confluence and could not be successfully passaged (**Figure 5A)**; thus when bulk cells are placed

in culture to derive CAF lines FH cells will outcompete FL cells over time due to their growth advantage. We therefore sought alternative culture conditions for FL cells; based on the expression of some genes related to adipogenesis in our FL population (e.g. *DLK1*, *PPARG*), we tested commercially available pre-adipocyte media and found that this media supported the expansion of FL cells over multiple passages (**Figure 5B)**. qRT-PCR analysis of FH and FL genes indicated that FL cells continued to express FL genes (*TCF21* and *DLK1*) at very high levels for up to 8 passages. However, we did see a decrease in these genes with increasing passage number, suggesting that even in pre-adipocyte media FL cells drift towards a FH phenotype with increasing time in culture (**Figure 5C**). We also saw an increase in *FAP* and *SULF1* gene expression with passage in some cases (**Figure 5C).** Thus to carry out the functional assays described below it was necessary to repeatedly isolate FL cells from patient samples and use them at passage 5 or less.

FH cells promote more gel contraction, cancer cell invasion and chemotherapy resistance than FL cells

A hallmark of CAFs is their ability to contract collagen gels (Ngo et al., 2006). Notably, two early passage FH CAF lines (851FH and 68425FH) showed a greater ability to contract collagen gels than two early passage FL CAF lines (507FL and 598FL; **Figure 5D**). Another property commonly attributed to CAFs is the ability to promote cancer cell invasion (Goetz et al., 2011; Kalluri, 2016; Karnoub et al., 2007). To compare the ability of FH and FL CAFs to promote invasion, spheroids were established with GFP-expressing HGSOC cell lines OVCAR8, ES2 and OV90, either alone or together with FH CAFs or FL CAFs at a ratio of 5:1 (CAFs:cancer cells). The spheroids were embedded in Matrigel and imaged by fluorescence microscopy after a period of incubation at 37°C that was optimized for individual cell lines and different batches of Matrigel (**Figure S5A)**. For OVCAR8, and OV90 invasion was quantified by measuring the circularity of at least 5 spheroids per condition; a decrease in circularity is indicative of cells invading into the Matrigel, generating branches radiating away from the spheroids and thus causing spheroids to deviate from a circular shape. The invasion pattern of ES2 cells was distinct and consisted of individual cells migrating outwards into the Matrigel, rather than formation of branches. Invasion was therefore quantified by counting the number of cells outside of the sphere, rather than measuring circularity. Upon testing of FH and FL CAFs from multiple patients, FH CAFs had an overall significantly greater ability to promote the invasion of OVCAR8, ES2 and OV90 cells

compared to FL CAFs. Notably, in cases where it was possible to assess patient-matched FH and FL CAFs (Patient 438 on all 3 cell lines; patient 598 on ES2 cells) there was a statistically significant difference, with FH CAFs inducing more invasion than FL CAFs (**Figure 5E**).

The standard of care for patients with HGSOC includes treatment with platinum-based chemotherapy, and chemo-resistance is a major factor leading to poor outcome in this disease. We determined the IC50s for carboplatin in OVCAR8, ES2 and OV90 cells growing under adherent conditions on plastic and showed that they ranged from 6 to 24 μM at 5 days after treatment (**Figure S6A**). Based on this information, subsequent experiments were performed using 10 μM carboplatin. To determine if FH and/or FL CAFs could influence cancer cell responses to chemotherapy, GFP-labelled OVCAR8, ES2 or OV90 cells were seeded onto feeder layers of FH CAFs or FL CAFs in flat-bottom 96 well plates. The next day 10 μM carboplatin was added and cells were cultured for an additional 10 days. GFP+ cancer cells were quantified daily using an Incucyte Zoom live cell imaging system. Both OVCAR8 and ES2 cells were rendered more resistant to carboplatin treatment in the presence of FH CAFs compared to FL CAFs, as indicated by more robust growth and a larger number of cells remaining at the end of the 10-day treatment period in FH co-cultures (**Figure 5F**). This included two pairs of patient-matched FH and FL CAFs (598FH and FL; 438FH and FL) that showed distinct outcomes. OV90 cells did not display any differences. Notably, for the two separate batches of experiments performed (**Figure 5F**) 851FH CAFs were used in both, and displayed very reproducible growth curves in all three cell lines.

FH CAFs promote *in vivo* tumor growth and metastasis to lymph nodes.

To ask if FH and FL CAFs have distinct influences over cancer cell behavior *in vivo*, we generated spheroids as above using luciferase-tagged OVCAR8 cells and implanted single spheroids into the mammary fat pads of non-obese diabetic/severe combined immunodeficient/IL2R-γ double-knockout (NSG) mice (**Figure S5B**). We implanted spheroids into the mammary fat pad due to earlier work by our group showing more efficient HGSOC tumor growth at this site (Stewart et al., 2011). Tumor growth was monitored by serial imaging of luciferase activity (**Figure 6A**). Of 10 mice implanted in each group take rates were 6/10, 5/10, 6/10 and 9/10 for the no CAF control, 363FL CAFs, 374FL CAFs and 851FH CAFs, respectively, suggesting a possible enhancement of take rate in spheroids containing FH CAFs, although differences did not reach statistical significance. Tumors that contained FH CAFs (851FH) grew

more rapidly compared to tumors containing FL CAFs (363FL or 374FL; **Figure 6B)**. Furthermore, 4 of 10 mice in the FH group had axillary lymph node or abdominal metastases compared to 0 of 5 mice and 1 of 6 mice the two FL groups and 1 of 6 mice in the no CAF control group (**Figure 6C).** Importantly, this held true when the mice injected with FL CAF-containing spheroids were maintained for an additional 3 weeks, allowing the size of their tumors to reach a size exceeding the FH tumors at week 8, indicating that the difference in metastasis was not simply a function of larger tumor size in the FH group.

Overexpression of TCF21 in FH CAFs decreases their pro-tumorigenic phenotype.

TCF21 is the most highly expressed transcription factor in FL CAFs and is essential for the formation of cardiac fibroblasts during embryonic development (Acharya et al., 2012). TCF21 has differentiation inhibiting function in skeletal muscle and smooth muscle cells (Braitsch et al., 2012; Funato et al., 2003; Nurnberg et al., 2015) and is also highly expressed in white adipose tissues (de Jong et al., 2015). Because lipid metabolism, ventricular development and cardiac related pathways were enriched in FL CAFs (**Figure 3D**), we hypothesized that TCF21 might be a master regulator of FL CAF identity. To test this possibility, 851FH CAFs were transduced with lentiviral vectors expressing either TCF21 and GFP (851FH-TCF21) or GFP alone (851FH-GFP) and GFP+ cells were FACS-purified and briefly expanded. TCF21 expression was validated by qRT-PCR and Western blot (**Figure 7A**). We then compared the functional properties of 851FH-TCF21 and 851FH-GFP cells. 851FH-TCF21 CAFs grew preferentially in preadipocyte media compared to 10% FBS media (data not shown), and the ability of 851FH-TCF21 CAFs to contract collagen gels was decreased in comparison to 851FH-GFP cells (**Figure 7B).** The spheroid invasion assay was carried out using mCherry labelled OVCAR8 and OV90 cells (because the 851FH-TCF21 and 851FH-GFP CAFs were GFP+), allowing imaging of both cancer and CAF cells in this assay. The invasion of both cell types was significantly reduced upon overexpression of TCF21 in 851FH CAFs (**Figure 7C).** We next carried out co-cultures of OVCAR8, OV90 and ES2 cells with 851FH-TCF21 or 851FH-GFP CAFs in the presence of 10 μM carboplatin. OVCAR8 and ES2 cells grew more robustly in co-cultures with 851FH-GFP CAFs than in co-cultures with 851FH-TCF21 CAFs, suggesting that TCF21 expression reduced the ability of 851FH CAFs to promote the survival of cancer cells in the presence of carboplatin (**Figure 7D**). Once again, no effect was seen with OV90 cells. Finally, heterospheroids composed of OVCAR8

cancer cells and 851FH-TCF21 or 851FH-GFP fibroblasts were implanted in the mammary fat pad and growth was monitored by serial imaging of luciferase activity (**Figure 7E**). Both 851FH-TCF21 and 851FH-GFP accelerated tumor growth compared to OVCAR8 cells alone. Tumors were significantly larger in the 851FH-GFP cohort at the 2-week time point, but not at the 4 and 6-week time points (**Figure 7F**).

DISCUSSION

The identification of distinct CAF subtypes in HGSOC that we describe here was facilitated by the identification of CD49e as a pan-fibroblast marker and the resulting ability to profile CAFs isolated directly from primary tumor specimens. Unsupervised clustering of genome-wide expression data then revealed, in an unbiased manner, the presence of heterogeneity within the fibroblast population. Subsequent validation steps confirmed that FAP expression within the CD49e+ subset is heterogeneous and that FH and FL CAFs are isolatable. Furthermore, RNAseq on isolated FH and FL CAFs demonstrated that, regardless of which population is predominant in a given tumor, the subtypes cluster with each other once isolated and have distinct transcriptional profiles. We then went on to demonstrate that patients with predominantly FH CAFs in their stroma, as determined either by detection of a FH CAF-specific gene signature or by flow cytometry, have shorter disease-free and/or overall survival. Functional assays demonstrated that FH CAFs influence cancer cells in a variety of ways, including promotion of invasion, resistance to carboplatin, and proliferation and metastasis *in vivo*, thus explaining the negative role that this CAF subtype plays in patient outcomes. By contrast, FL CAFs do not appear to promote these behaviors in cancer cells. In summary, we demonstrate that CAFs in HGSOC are heterogeneous and that different subtypes have distinct influences on cancer aggressiveness and patient outcomes.

IF on large tissue sections showed that the two CAF subtypes can be located in distinct regions of the tumor tissue. This raises the concern that there is regional heterogeneity in CAF phenotype within a single tumor sample such that a different result may be obtained depending on where in the tumor a particular sample was obtained. Our analysis by flow cytometry as well as the TCGA analysis of bulk tumor samples by RNAseq, appeared to contain a sufficient representation of the average CAF content within a sample, given that the results were predictive of patient outcomes. However, it is important to be aware that both flow cytometry and RNA-seq provide an overall average of the proportion of FH/FL CAFs within a sample and cannot provide

information on regional heterogeneity. This would be of particular concern if small biopsies are being analyzed, and additional studies in which different regions of tumor specimens are analyzed will be important to further clarify intra-tumoral CAF heterogeneity in the future.

While it has been known for some time that CAFs are heterogeneous (Kalluri, 2016; Ohlund et al., 2014; Sugimoto et al., 2006), only recently have distinct CAF subtypes begun to be identified and characterized. For example, a recent study showed that CAFs in close proximity to cancer cells in pancreatic cancer are αSMA+ myofibroblasts, whereas fibroblasts more distant from cancer cells lack elevated αSMA and instead secrete inflammatory cytokines (Ohlund et al., 2017). A CAF subset defined by expression of CD10 and GPR77 varied in frequency in breast and lung cancers and was associated with resistance to chemotherapy and shorter patient survival (Su et al., 2018). Importantly, in both of these studies the identified subtypes were all FAP-positive, suggesting that they represent heterogeneity within the FH fraction. An additional study of breast cancer used multiple fibroblast markers to identify 4 CAF subsets, of which only one was FAP-positive ("S1") and 3 were FAP-negative ("S2-S4"; Costa et al., 2018). Interestingly, the "S1" and "S4" subtypes were associated with aggressive HER2 and triple negative breast cancers, and triple negative breast cancer could be divided into two subgroups based on the presence of either S1 or S4 CAF subtypes. In a separate study the same group identified S1 and S4 CAFs in HGSOC (Givel et al., 2018). They showed that "mesenchymal" samples are enriched for S1 CAFs, suggesting that S1 CAFs resemble our FH CAFs. However, the other CAF subtypes identified in this study were not further profiled, thus we cannot determine if any of these are the same or similar to FL CAFs. Overall however, these recent studies are supportive of our observation that FH and FL CAFs represent distinct CAF subtypes within HGSOC, while our study is the first to describe their isolation and molecular and functional characterization. Future studies will be needed to determine if further heterogeneity exists within HGSOC CAFs, for example using single cell RNA-Seq.

The studies by (Givel et al., 2018) and (Costa et al., 2018) showed that FAP-positive CAFs have immunosuppressive functions in HGSOC and breast cancer. Other studies have also demonstrated an immune-suppressive function of FAP-expressing stromal cells (Fearon, 2014; Kraman et al., 2010; Yang et al., 2016). We find a large cluster of pathways involved in immune regulation in FH CAFs (Figure 3D, Table S4A), which include many chemokines and cytokines involved in immune processes such as generation of myeloid-derived suppressor cells (e.g. *CXCL12*, *IL11*, *VEGF*), macrophage polarization (e.g. *CXCL12*, *IL10*, *Chi3L1*), differentiation of

immune suppressive T regulatory cells (e.g. *IL1B*, *IL10*, *IL11*) and inhibition of CD8+ cytotoxic T cells (e.g. *PDCD1LG2*, *LGALS1*). Future work will include a focus on immune subtypes present in FH *vs* FL patients and understanding the cross-talk between subtypes of CAFs and immune cells in this cancer. By contrast, the FL CAFs have a distinct gene expression profile that lacks the secretory phenotype seen in FH cells. Prominent networks include translation/protein localization, ion transport/cardiac muscle contraction, and lipid metabolism and steroid biosynthesis. The latter is in agreement with our finding that FL cells grew preferentially in pre-adipocyte media, which contains low serum plus supplements that include EGF and compounds that are pro-adipogenic such as dexamethasone, 3-isobutyl-1-methylxanthine (IBMX) and ciglitazone, a PPARγ agonist. However, the prominent muscle contraction network suggests that these cells may have a more primitive mesenchymal progenitor phenotype that has both myogenic and adipogenic potential. Comparison of the FL gene signature to published mesenchymal stem cell (MSC) signatures, however, suggests that these cells are not MSCs. Indeed, MSCs more closely resemble FH CAFs as they have elevated expression of FAP as well as multiple ECM proteins and ECM remodeling enzymes (Jeong et al., 2005; Wagner et al., 2005), thus further investigations, including functional assays, will be required to better elucidate the origin and/or identity of FL CAFs. For example, it will be of interest in the future to compare the abilities of FH and FL CAFs to differentiate into various mesenchymal lineages and to determine if additional manipulations of the culture conditions can identify a condition that can maintain FL CAFs indefinitely *in vitro*.

Altogether, our functional assays suggest that the worse survival outcomes of patients with a FH gene signature and/or a predominance of FH CAFs within their stroma are mediated by CAF-cancer cell interactions that promote cancer cell proliferation, invasion, and therapy resistance, as well as immune-suppression as shown by others (Givel et al., 2018). There was some variability between individual FH CAF lines in their ability to influence these properties, and also variability in cell lines in their responses (e.g., the carboplatin response of OV90 cells was not affected by FH CAFs). This result suggests different mechanisms for each of the induced behaviors, as well as different responses between individual tumors. In spite of this variation, our results indicate that future studies focused on targeting FH CAFs in order to improve outcomes and/or responses to standard chemotherapy or immunotherapy are warranted.

The unique transcriptional programs of FH and FL CAFs prompted us to more closely examine differentially expressed transcription factors between the two CAF subtypes and TCF21

was the most highly differentially expressed transcription factor in FL cells. TCF21 is expressed in epicardial progenitor cells that give rise to coronary artery smooth muscle cells and cardiac fibroblasts (Nurnberg et al., 2015), the latter of which are a source of activated myofibroblasts in the infarcted heart (Kanisicak et al., 2016). TCF21 is also a marker for white adipose tissue and is abundantly expressed in visceral fat-derived stem cells (Akama and Chun, 2018). When we overexpressed TCF21 in FH CAFs, we saw a reduction in gel contraction, as well as a decrease in CAF-induced invasion in our 3-D spheroid invasion assay, and a decrease in the ability of FH CAFs to promote the survival of cancer cells in 2 of the 3 cell lines tested. We also saw a slight delay in tumor growth *in vivo*. These results suggest that TCF21 on its own can dampen the ability FH CAFs to promote gel contraction, invasion, chemo-resistance and *in vivo* tumor growth, but additional transcription factors or co-regulators of TCF21 and/or epigenetic regulators of chromatin accessibility are likely required to completely reprogram FH CAFs to a state that lacks pro-tumorigenic properties. Future epigenomic profiling studies will be required to compare the epigenetic states of FH and FL CAFs and identify potential avenues to "reprogram" FH CAFs to a state that is not supportive of cancer cell invasion, chemoresistance or immune suppression.

ACKNOWLEDGEMENTS

We thank the UHN Program for Biospecimen Sciences for fresh tissue acquisition, and the UHN Animal Resources Centre staff for animal care. This work was supported by grants from the Canadian Institutes of Health Research to (PJT153147, MOP137087), the Ontario Institute for Cancer Research (Investigator Award) and the Princess Margaret Cancer Foundation, thanks to the generosity of the Westaway Charitable Foundation. AH was supported by Ontario Student Opportunity Trust Funds and Medical Biophysics Excellence awards.

AUTHOR CONTRIBUTIONS

Conceptualization, A.H., L.E.A and B.G.N..; Methodology, A.H. and L.E.A.; Investigation, A.H., S.P., J.D., J.M. and J.P; Resources, V.W.H., K.H.T., B.C. and M.Q.B.; Formal Analysis, V.V., G.D.B.; Writing – Original Draft, A.H. and L.E.A.; Writing – Review & Editing, A.H., V.V., B.G.N. and L.E.A.; Supervision, B.G.N., G.D.B. and L.E.A.; Funding Acquisition, L.E.A.

DECLARATION OF INTERESTS

The authors declare no competing interests.

REFERENCES

Acharya, A., Baek, S.T., Huang, G., Eskiocak, B., Goetsch, S., Sung, C.Y., Banfi, S., Sauer, M.F., Olsen, G.S., Duffield, J.S., *et al.* (2012). The bHLH transcription factor Tcf21 is required for lineage-specific EMT of cardiac fibroblast progenitors. Development *139*, 2139-2149.

Akama, T., and Chun, T.H. (2018). Transcription factor 21 (TCF21) promotes proinflammatory interleukin 6 expression and extracellular matrix remodeling in visceral adipose stem cells. J Biol Chem *293*, 6603-6610.

Braitsch, C.M., Combs, M.D., Quaggin, S.E., and Yutzey, K.E. (2012). Pod1/Tcf21 is regulated by retinoic acid signaling and inhibits differentiation of epicardium-derived cells into smooth muscle in the developing heart. Dev Biol *368*, 345-357.

Carter, S.L., Cibulskis, K., Helman, E., McKenna, A., Shen, H., Zack, T., Laird, P.W., Onofrio, R.C., Winckler, W., Weir, B.A., *et al.* (2012). Absolute quantification of somatic DNA alterations in human cancer. Nat Biotechnol *30*, 413-421.

Costa, A., Kieffer, Y., Scholer-Dahirel, A., Pelon, F., Bourachot, B., Cardon, M., Sirven, P., Magagna, I., Fuhrmann, L., Bernard, C., *et al.* (2018). Fibroblast Heterogeneity and Immunosuppressive Environment in Human Breast Cancer. Cancer Cell *33*, 463-479 e410.

Fearon, D.T. (2014). The carcinoma-associated fibroblast expressing fibroblast activation protein and escape from immune surveillance. Cancer Immunol Res *2*, 187-193.

Funato, N., Ohyama, K., Kuroda, T., and Nakamura, M. (2003). Basic helix-loop-helix transcription factor epicardin/capsulin/Pod-1 suppresses differentiation by negative regulation of transcription. J Biol Chem *278*, 7486-7493.

Gedye, C.A., Hussain, A., Paterson, J., Smrke, A., Saini, H., Sirskyj, D., Pereira, K., Lobo, N., Stewart, J., Go, C., *et al.* (2014). Cell surface profiling using high-throughput flow cytometry: a platform for biomarker discovery and analysis of cellular heterogeneity. PLoS One *9*, e105602.

Givel, A.M., Kieffer, Y., Scholer-Dahirel, A., Sirven, P., Cardon, M., Pelon, F., Magagna, I., Gentric, G., Costa, A., Bonneau, C., *et al.* (2018). miR200-regulated CXCL12beta promotes fibroblast heterogeneity and immunosuppression in ovarian cancers. Nat Commun *9*, 1056.

Goetz, J.G., Minguet, S., Navarro-Lerida, I., Lazcano, J.J., Samaniego, R., Calvo, E., Tello, M., Osteso-Ibanez, T., Pellinen, T., Echarri, A., *et al.* (2011). Biomechanical remodeling of the microenvironment by stromal caveolin-1 favors tumor invasion and metastasis. Cell *146*, 148-163.

Hamanishi, J., Mandai, M., Ikeda, T., Minami, M., Kawaguchi, A., Murayama, T., Kanai, M., Mori, Y., Matsumoto, S., Chikuma, S., *et al.* (2015). Safety and Antitumor Activity of Anti-PD-1 Antibody, Nivolumab, in Patients With Platinum-Resistant Ovarian Cancer. J Clin Oncol *33*, 4015-4022.

Jeong, J.A., Hong, S.H., Gang, E.J., Ahn, C., Hwang, S.H., Yang, I.H., Han, H., and Kim, H. (2005). Differential gene expression profiling of human umbilical cord blood-derived mesenchymal stem cells by DNA microarray. Stem Cells *23*, 584-593.

Junttila, M.R., and de Sauvage, F.J. (2013). Influence of tumour micro-environment heterogeneity on therapeutic response. Nature *501*, 346-354.

Kalluri, R. (2016). The biology and function of fibroblasts in cancer. Nat Rev Cancer *16*, 582-598.

Kalluri, R., and Zeisberg, M. (2006). Fibroblasts in cancer. Nat Rev Cancer *6*, 392-401.

Kanisicak, O., Khalil, H., Ivey, M.J., Karch, J., Maliken, B.D., Correll, R.N., Brody, M.J., SC, J.L., Aronow, B.J., Tallquist, M.D.*, et al.* (2016). Genetic lineage tracing defines myofibroblast origin and function in the injured heart. Nat Commun *7*, 12260.

Karnoub, A.E., Dash, A.B., Vo, A.P., Sullivan, A., Brooks, M.W., Bell, G.W., Richardson, A.L., Polyak, K., Tubo, R., and Weinberg, R.A. (2007). Mesenchymal stem cells within tumour stroma promote breast cancer metastasis. Nature *449*, 557-563.

Kobel, M., Piskorz, A.M., Lee, S., Lui, S., LePage, C., Marass, F., Rosenfeld, N., Mes Masson, A.M., and Brenton, J.D. (2016). Optimized p53 immunohistochemistry is an accurate predictor of TP53 mutation in ovarian carcinoma. J Pathol Clin Res *2*, 247-258.

Kraman, M., Bambrough, P.J., Arnold, J.N., Roberts, E.W., Magiera, L., Jones, J.O., Gopinathan, A., Tuveson, D.A., and Fearon, D.T. (2010). Suppression of antitumor immunity by stromal cells expressing fibroblast activation protein-alpha. Science *330*, 827-830.

Kuzet, S.E., and Gaggioli, C. (2016). Fibroblast activation in cancer: when seed fertilizes soil. Cell Tissue Res *365*, 607-619.

Ledermann, J.A., Raja, F.A., Fotopoulou, C., Gonzalez-Martin, A., Colombo, N., Sessa, C., and Group, E.G.W. (2013). Newly diagnosed and relapsed epithelial ovarian carcinoma: ESMO Clinical Practice Guidelines for diagnosis, treatment and follow-up. Ann Oncol *24 Suppl 6*, vi24-32.

Mhawech-Fauceglia, P., Yan, L., Sharifian, M., Ren, X., Liu, S., Kim, G., Gayther, S.A., Pejovic, T., and Lawrenson, K. (2015). Stromal Expression of Fibroblast Activation Protein Alpha (FAP) Predicts Platinum Resistance and Shorter Recurrence in patients with Epithelial Ovarian Cancer. Cancer microenvironment : official journal of the International Cancer Microenvironment Society *8*, 23-31.

Monk, B.J., Minion, L.E., and Coleman, R.L. (2016). Anti-angiogenic agents in ovarian cancer: past, present, and future. Ann Oncol *27 Suppl 1*, i33-i39.

Moore, K., Colombo, N., Scambia, G., Kim, B.G., Oaknin, A., Friedlander, M., Lisyanskaya, A., Floquet, A., Leary, A., Sonke, G.S.*, et al.* (2018). Maintenance Olaparib in Patients with Newly Diagnosed Advanced Ovarian Cancer. N Engl J Med *379*, 2495-2505.

Ngo, P., Ramalingam, P., Phillips, J.A., and Furuta, G.T. (2006). Collagen gel contraction assay. Methods Mol Biol *341*, 103-109.

Nurnberg, S.T., Cheng, K., Raiesdana, A., Kundu, R., Miller, C.L., Kim, J.B., Arora, K., Carcamo-Oribe, I., Xiong, Y., Tellakula, N.*, et al.* (2015). Coronary Artery Disease Associated Transcription Factor TCF21 Regulates Smooth Muscle Precursor Cells That Contribute to the Fibrous Cap. PLoS Genet *11*, e1005155.

Ohlund, D., Elyada, E., and Tuveson, D. (2014). Fibroblast heterogeneity in the cancer wound. J Exp Med *211*, 1503-1523.

Ohlund, D., Handly-Santana, A., Biffi, G., Elyada, E., Almeida, A.S., Ponz-Sarvise, M., Corbo, V., Oni, T.E., Hearn, S.A., Lee, E.J.*, et al.* (2017). Distinct populations of inflammatory fibroblasts and myofibroblasts in pancreatic cancer. J Exp Med *214*, 579-596.

Ryner, L., Guan, Y., Firestein, R., Xiao, Y., Choi, Y., Rabe, C., Lu, S., Fuentes, E., Huw, L.Y., Lackner, M.R., *et al.* (2015). Upregulation of Periostin and Reactive Stroma Is Associated with Primary Chemoresistance and Predicts Clinical Outcomes in Epithelial Ovarian Cancer. Clinical cancer research : an official journal of the American Association for Cancer Research *21*, 2941-2951.

Stewart, J.M., Shaw, P.A., Gedye, C., Bernardini, M.Q., Neel, B.G., and Ailles, L.E. (2011). Phenotypic heterogeneity and instability of human ovarian tumor-initiating cells. Proc Natl Acad Sci U S A *108*, 6468-6473.

Su, S., Chen, J., Yao, H., Liu, J., Yu, S., Lao, L., Wang, M., Luo, M., Xing, Y., Chen, F., *et al.* (2018). CD10(+)GPR77(+) Cancer-Associated Fibroblasts Promote Cancer Formation and Chemoresistance by Sustaining Cancer Stemness. Cell *172*, 841-856 e816.

Sugimoto, H., Mundel, T.M., Kieran, M.W., and Kalluri, R. (2006). Identification of fibroblast heterogeneity in the tumor microenvironment. Cancer Biol Ther *5*, 1640-1646.

Thibault, B., Castells, M., Delord, J.P., and Couderc, B. (2014). Ovarian cancer microenvironment: implications for cancer dissemination and chemoresistance acquisition. Cancer metastasis reviews *33*, 17-39.

Verhaak, R.G., Tamayo, P., Yang, J.Y., Hubbard, D., Zhang, H., Creighton, C.J., Fereday, S., Lawrence, M., Carter, S.L., Mermel, C.H., *et al.* (2013). Prognostically relevant gene signatures of high-grade serous ovarian carcinoma. J Clin Invest *123*, 517-525.

Wagner, W., Wein, F., Seckinger, A., Frankhauser, M., Wirkner, U., Krause, U., Blake, J., Schwager, C., Eckstein, V., Ansorge, W., *et al.* (2005). Comparative characteristics of mesenchymal stem cells from human bone marrow, adipose tissue, and umbilical cord blood. Exp Hematol *33*, 1402-1416.

Yang, X., Lin, Y., Shi, Y., Li, B., Liu, W., Yin, W., Dang, Y., Chu, Y., Fan, J., and He, R. (2016). FAP Promotes Immunosuppression by Cancer-Associated Fibroblasts in the Tumor Microenvironment via STAT3-CCL2 Signaling. Cancer Res *76*, 4124-4135.

Yeung, T.L., Leung, C.S., Li, F., Wong, S.S., and Mok, S.C. (2016). Targeting Stromal-Cancer Cell Crosstalk Networks in Ovarian Cancer Treatment. Biomolecules *6*.

Yoshihara, K., Shahmoradgoli, M., Martinez, E., Vegesna, R., Kim, H., Torres-Garcia, W., Trevino, V., Shen, H., Laird, P.W., Levine, D.A., *et al.* (2013). Inferring tumour purity and stromal and immune cell admixture from expression data. Nat Commun *4*, 2612.

Zhang, S., Jing, Y., Zhang, M., Zhang, Z., Ma, P., Peng, H., Shi, K., Gao, W.Q., and Zhuang, G. (2015). Stroma-associated master regulators of molecular subtypes predict patient prognosis in ovarian cancer. Sci Rep *5*, 16066.

FIGURE LEGENDS

Figure 1. Prospective isolation and transcriptional profiling of CAFs from primary HGSOC samples.

(A) Representative images of immunofluorescence on 5 different HGSOC samples using pan-cytokeratin (CK; red) and CD49e (green) antibodies. Scale bar = 100 µm. See also Figure S1.

(B) Representative FACS plots from 6 different patients showing the viable, CD45-CD31- population stained for EpCAM and CD49e.

(C) Representative images of cytospins made from isolated EpCAM+ or CD49e+ cells stained for pan-CK (red), Vimentin (green), and Hoechst (blue). Scale bar = 50 µm.

(D) Representative images of cytospins made from isolated EpCAM+ or CD49e+ cells stained for p53 (red) and Hoechst (blue). Scale bar = 50 µm.

(E) Heatmap showing unsupervised hierarchical clustering of CD49e+ and EpCAM+ cells isolated directly from HGSOC tumor specimens and profiled by Illumina HT-12v4 microarrays. The EpCAM+ cells were separated into CD133+ and CD133- fractions. The heatmap shows EpCAM+ populations from 12 patients and CD49e+ samples from 10 patients due to data being of poor quality from two of the CD49e+ samples. See also Figure S2A.

(F) Gene set enrichment analysis of the genes differentially expressed in the CD49e+ *vs* EpCAM+ populations. The top 20 non-redundant gene sets for each population are shown. See also Tables S2A and S2B.

Figure 2. Identification of FH and FL CAFs in HGSOC.

(A) Heatmap of the top 500 genes differentially expressed between FH and FL subtypes contained within the CD49e+ fraction (left), and analysis of the same gene list in the Leung *et al* HGSOC and normal ovary stromal samples obtained by laser capture microdissection (right). Black bar: tumor stroma; Blue bar: normal stroma. Black dendrogram: FH patients; Red dendrogram: FL patients. *FAP* gene expression is shown enlarged at the bottom of the heatmap. See also Figure S2 and Tables S3A and S3B.

(B) RNA from the CD49e+ fraction of 3 FH tumors and 3 FL tumors (as classified by microarray) was analyzed by qRT-PCR for the expression of 3 FH-specific genes and 3 FL-specific genes. Mean±SEM, n=3. *$p<0.05$; **$p<0.01$; ****$p<0.0001$.

(C) Representative images of HGSOC serial tissue sections stained with antibodies to FAP or TCF21. All sections were co-stained for pan-CK to delineate epithelial and stromal regions and Hoechst to stain nuclei. HALO image analysis software was used to quantify antibody staining within the pan-CK negative stromal regions. Images show the stained sections with the HALO analysis mask, where epithelial cells are shown in red, nuclei within the stromal region are white, and FAP or TCF21 positive cells are yellow. Scale bar = 50 μm. See also Figure S3 for additional images.

(D) Serial sections from patient 70535 stained for FAP or TCF21 are shown. White outline indicates a FAP-high/TCF21-low region and red outline indicates a FAP-low/TCF21-high region within a single tissue section. Scale bar = 200 μm.

(E) Graph comparing the % stromal area positive for FAP and TCF21 within the entire tissue section, for 5 tumors analyzed.

(F) Quantification of the proportion of FH cells within the viable CD45-CD31-EpCAM-CD49e+ fraction by flow cytometry in 64 primary samples and 2 matched recurrences. 3 representative FACS plots, gated on the CD45-CD31-EpCAM-CD49e+ cells and showing FAP staining, are shown above the graph. Gates were set based on a fluorescence-minus-one control for FAP. The two matched primary (P) and recurrent (R) samples are indicated below the graph.

(G) Graph comparing FAP quantification data obtained using flow cytometry and IF for samples that were analyzed using both methods.

Figure 3. Transcriptional profiling of purified FH and FL CAFs.

(A) Principal components analysis of RNA-Seq data from FACS-purified FH and FL cells. Dotted lines indicate cases for which FH and FL cells were purified from the same tumor specimen.

(B) Gene set enrichment analysis of the FH (left) and FL (right) gene lists generated from RNA-Seq data in comparison to the gene lists previously generated by microarrays.

(C) Scatter plots of FH *vs* FL gene expression in the 3 patients where both populations were isolated from the same patient. The three FH and three FL genes previously used for validation are indicated as gray dots.

(D) Cytoscape map of the most significantly differentially expressed gene ontology (GO) terms and pathways between FH and FL CAFs. GSEA was performed and the top 300 most differentially

expressed GO terms and Reactome pathways are shown. The size of individual nodes correlates with the number of genes in each.
See also Tables S4A and S4B.

Figure 4. FH patients correspond to the mesenchymal molecular subtype and have worse clinical outcomes than FL patients.

(A) Heatmap of TCGA HGSOC data showing unsupervised clustering of patients using the FH- and FL-specific CAF gene lists. The TCGA molecular subtypes (Verhaak et al., 2013) are shown above the heatmap in blue. Patients expressing either 75% or 50% of the FH signature genes are indicated in black and gray, respectively. Patients expressing either 75% or 50% of the FL signature genes are indicated in red and pink, respectively.
(B) GSEA comparing the FH (left) and FL (right) gene lists to the genes expressed in TCGA mesenchymal subtype.
(C) The ABSOLUTE (left) and ESTIMATE (right) algorithms were applied to patients falling into the FH (black), FL (red) and "other" (blue) categories of patients selected using the more stringent 75% cut-off.
(D) Kaplan-Meier survival curves of patients falling into the FH (n=80) and FL (n=30) groups (based on the 75% cut-off). Median overall survival was 3.3 years for FH and 5.7 years for FL patients. Median disease-free survival was 1.2 years for FH and 2.1 years for FL patients.
(E) Kaplan-Meier survival curve of patients from our centre that were profiled by flow cytometery for the proportion of CD49e+ CAFs that were positive for FAP staining. Patients were separated into FH and FL based on the median FAP expression (See Table S1). Recurrence was scored when CA125 levels rose above 35 U/ml. The median time to recurrence was 1.7 years for FH and 3.4 years for FL patients.
See also Figure S4, Table S1 and Table S5.

Figure 5. FH and FL CAFs have distinct functional properties.

(A) Growth curves of isolated FH and FL CAFs from 3 patients cultured in 10% FBS. Mean±SEM, n=3. **p<0.01, ***p<0.001, two-way ANOVA.
(B) Pre-adipocyte media is supportive of FL cells, allowing them to be grown to confluence and passaged. Scale bar = 50 μm

(C) qRT-PCR for FH genes (FAP, SULF1) and FL genes (TCF21, DLK1) in passaged FL cells (red; passage # indicated below each bar). A cultured patient-derived CAF line was used as a control (black bar). Fold-differences in gene expression were determined using the ΔΔ-Ct method, using *UBC* as a housekeeping gene, with 3 technical replicates per sample assayed.

(D) Representative images of collagen gels cultured for 36 hours with two FH derived CAF lines and two FL-derived CAF lines (left); quantification of gel contraction over time (right). Mean ± SEM, n=4. P-values for comparisons between FH and FL lines ranged from 0.02 to 0.002, two-way ANOVA. Scale bar = 500 µm

(E) Representative images of spheroids generated using GFP-expressing HGSOC cell lines OVCAR8, ES2 or OV90 combined with FH or FL fibroblasts (left). Spheroids were embedded in Matrigel and imaged after 1 (for ES2) to 4 (for OVCAR8 and OV90) days. Circularity was quantified using Image J for OVCAR8 and OV90 cells; the number of cells outside the spheroid was quantified using Image J for ES2 cells (right). Data is normalized to spheroids containing no CAFs. Mean±SEM, n=5 to 10 spheroids per condition. P-values calculated using Student's t-test. Scale bar = 50 µm. [#]The difference between 438FL and 68425FH in OVCAR8 cells was not significant. See also Figure S5A.

(F) Growth curves of GFP-labelled cancer cells co-cultured with FH or FL CAFs after treatment with 10 µM carboplatin. Experiments were done in two separate batches ("Set 1" and "Set 2"). CAF line 851FH was used in both experiments. Data was normalized to the GFP+ area at Day 0. Mean±SEM, n=3. Asterisks reflect differences at the end of 10 days. **p<0.01, ****p<0.0001, Student's t-test. See also Figure S6.

Figure 6. FH but not FL CAFs promote *in vivo* tumor growth and metastasis.

(A) Spheroids of luciferase-expressing OVCAR8 cells alone or combined with FH or FL CAFs were generated as for invasion assays. After 72 hours of spheroid formation, individual spheroids were implanted into the mammary fat pads of NSG mice. Tumor growth was monitored over time using the Xenogen IVIS Imaging System 100. Representative images of a single mouse from each condition over time are shown. All mice were exposed for the same amount of time to allow visualisation of differences in tumor size over time. See also Figure S5B.

(B) Quantification of luciferase signal, normalized to an unimplanted mouse over a period of 8 weeks. Mean±SEM, n=5 to 10 (animals in which tumors failed to grow were not included). **p<0.01, two-way Anova *vs* control group.

(C) Average tumor sizes in each group at 8 weeks and 11 weeks post-implantation. Numbers above the bars indicate the number of mice with metastases over the total number of tumor-bearing mice in each group. Mean±SEM, n=5 to 10.

Figure 7. Overexpression of TCF21 in FH CAFs influences their functional properties.

(A) qRT-PCR (left) and Western blot (right) for TCF21 expression in 851FH-GFP and 851FH-TCF21 CAFs.

(B) Representative images of collagen gels cultured for 32 hours with 851FH-GFP CAFs or 851-TCF21 CAFs (left); quantification of gel contraction over time (right). Mean ± SEM, n=3. **p<0.01, two-way Anova. Scale bar = 500 µm

(C) Representative images of spheroids generated using mCherry-expressing HGSOC cell lines OVCAR8 or OV90 with 851FH-GFP or 851FH-TCF21 CAFs mixed in. Spheroids were embedded in Matrigel and imaged after 4 days (left). Circularity was quantified in both channels (green=CAFs, red = cancer cells) using Image J (right). Mean±SEM, n=10 spheroids per condition. *p<0.05, **p<0.01, ****p<0.0001, Student's t-test. Scale bar = 50 µm.

(D) Growth curves of mCherry-labelled cancer cells co-cultured with 851FH-GFP or 851FH-TCF21 CAFs after treatment with 10 µM carboplatin. Data was normalized to the mCherry+ area at Day 0. Mean±SEM, n=3. Asterisks reflect differences at the end of 10 days. ***p<0.001, ****p<0.0001, Student's t-test.

(E) Spheroids of luciferase-expressing OVCAR8 cells alone or with 851FH-GFP or 851FH-TCF21 CAFs mixed in were generated as for invasion assays. After 72 hours of spheroid formation, individual spheroids were implanted into the mammary fat pads of NSG mice. Representative images of individual mice are shown.

(F) Left: Quantification of luciferase signal, normalized to an unimplanted mouse over a period of 6 weeks. Mean±SEM, n=12. Right: Photon flux for individual tumors within the 851FH-GFP group *vs* the 851FH-TCF21 group at the 2 week and 6 week time points.

METHODS

Contact for Reagent and Resource Sharing

Further information and requests for resources and reagents should be directed to and will be fulfilled by the Lead Contact, Laurie Ailles (lailles@uhnresearch.ca).

Experimental Model and Subject Details

Patients and Tissue Samples

Tumor samples were obtained from 69 patients with high grade serous ovarian cancer who underwent surgery at the University Health Network (**Table S1**). All samples were collected from patients with informed consent, and all related procedures were performed with the approval of the Research Ethics Board of the University Health Network (Toronto, Canada).

Primary CAF Cultures

CAFs were derived from either bulk tumor cell suspensions or FACS purified cells (see detailed methods below). Bulk tumor cell suspensions were seeded into tissue culture plates in IMDM with 10% FBS. Fibroblasts adhered and grew out preferentially under these conditions over multiple passages. Fibroblast identity was verified based on cell morphology, as well as expression of Vimentin and lack of expression of Cytokeratin. CAFs were also verified to be negative for p53 staining (i.e. wild-type) in patients with positive p53 staining (i.e. mutant) in their tumor tissues. FH CAFs isolated by flow cytometry (Viable, CD45-, CD31-, EpCAM-, CD49e+, FAP-high) were seeded into wells of 96-well culture plates in IMDM with 10% FBS. FL CAFs isolated by flow cytometery (Viable, CD45-, CD31-, EpCAM-, CD49e+, FAP-low) were seeded into wells of 96-well culture plates in pre-adipocyte media (PromoCell). Cells were passaged 1:2 when they reached confluence using 0.25% Trypsin/1 mM EDTA. All CAF experiments were done at ≤ passage 10 for cultured CAFs and FH CAFs, and ≤ passage 5 for FL CAFs.

Cell Lines

Three HGSOC cell lines, OVCAR8, OV90 and ES2, were obtained from the ATCC and their identity was verified by Short Tandem Repeat (STR) profiling (AmpFℓSTR Identifiler, Life

Technologies), performed by The Centre for Applied Genomics, The Hospital for Sick Children, Toronto, Canada, and tested negative for *Mycoplasma* infection by MycoAlert (Lonza) according to the manufacturer's instructions. Lines were maintained as recommended by ATCC, as follows: OVCAR8 in IMDM with 10% FBS; ES2 in McCoy's 5A media with 10% FBS; OV90 in 1:1 M199:MCDB105 media with 15% FBS.

Mice

Female NOD/Lt-scid/IL2Rɣnull (NSG) mice were bred in-house at the University Health Network Animal Resources Centre. Spheroids were implanted into the fourth (inguinal) mammary fat pad on one side. Animal experiments were performed in accordance with national and institutional guidelines approved by the Canadian Counsel on Animal Care and approved by the University Health Network Animal Care Committee**.**

Method Details

Primary Tumor Dissociation

Bulk tumors were mechanically minced into a slurry with sterile scalpels and then enzymatically digested in Media 199 containing 300 U/ml Collagenase and 100 U/ml Hyaluronidase mixture (Stem Cell Technologies) and 125 U/ml DNAse-I (Cedarlane) for 1-2 hours at 37°C. Following digestion, samples were centrifuged at 350 x g for 5 minutes prior to treatment with 1-2ml of ACK lysing buffer (ThermoFisher Scientific) for 5 minutes on ice. Following red cell lysis, cells were pelleted, resuspended and filtered through a 70 µm sterile nylon mesh and viable cells defined by trypan blue exclusion. Cells were cryopreserved in 90% FBS/10% dimethyl sulfoxide.

High-Throughput Flow Cytometry (HT-FC)

HT-FC was performed on cultured CAFs and primary HGSOC tumor cell suspensions as previously described (Gedye et al., 2014). Briefly, 363 commercially available antibodies to cell surface antigens conjugated to PE, FITC or APC were aliquoted into round bottom 96-well plates, 2 µl per well into 48 µl of flow cytometry (FC) buffer (Hanks balanced salt solution + 2% FBS). Cell suspensions of 0.5 to 1 million cells/ml in FC buffer were aliquoted by multichannel pipette into pre-prepared HT-FC plates (50 µl per well), for a final volume of 100 µl per well and a final

antibody dilution of 1:50. Plates were incubated for 20 minutes on ice in the dark, centrifuged for 5 minutes at 350 x g, washed twice with 200 µl FC buffer, and resuspended in 50 to 80 µl FC buffer containing 0.1 µg/ml 4',6-diamidino-2-phenylindole (DAPI; Sigma-Aldrich). Primary tumor samples were stained with CD45-APC-Cy7 (Biolegend, 1:200) and CD31-PE-Cy7 (Biolegend, 1:200) prior to aliquoting into plates. Fluorescence-minus-one controls were generated for each fluorochrome used and compensations were set using BD Plus CompBeads and FACSDiva software. Data collection was performed on a Becton-Dickinson LSR II flow cytometer with ultraviolet (20mW), violet (25mW), blue (20mW) and red (17mW) lasers, with default filter configuration, utilizing the High Throughput Sampler attachment. At least 10,000 events were collected per well. The gating strategy based on fluorescence-minus-one controls is illustrated in Supplementary Figure S1B.

Flow Cytometry and FACS

Cryopreserved or fresh HGSOC single cell suspensions were washed and re-suspended at $\leq 1x10^7$ cell/ml in FC buffer and incubated with 10 µg/ml mouse IgG in FC buffer on ice for 10 min, followed by incubation with the following primary antibodies: CD45-PECy7 (BioLegend; 1:200), CD31-PECy7 (BioLegend; 1:200), CD49e-PE (BD Biosciences; 1:100), EpCAM-APC (BioLegend; 1:100). For experiments including CD133, an unconjugated mouse anti-human CD133 antibody was used (Miltenyi Biotec; 1:20), and for experiments including FAP, an unconjugated mouse anti-FAP antibody was used (R&D Systems; 1:50). Cells were incubated on ice for 15 minutes, washed and resuspended in FC buffer with goat-anti-mouse Alexa488 (Invitrogen; 1:400) for an additional 15 minutes, then washed and stained with the remaining directly conjugated antibodies as described above. Fluorescence-minus-one (FMO) controls were generated for each antibody and used as gating controls. Single-colour stained compensation beads (BD Biosciences) were used as compensation controls. Cells were analyzed on a BD LSR II flow cytometer or sorted using a BD FACS Aria.

Immunofluorescence

Cytospins

FACs-sorted cells were suspended in PBS+2% FBS at a concentration of $5x10^4$ cells/ml and 200 µl of cell suspension were spun onto each glass slide using a cytocentrifuge at 800 rpm for 5 minutes. Slides were air-dried, fixed in 100% ice cold acetone and air dried again. Cells were

permeabilized in Tris-buffered saline (TBS) containing 0.1% Tween for Cytokeratin and Vimentin, or 0.3% Triton X-100 for p53 (TBS-T) for 10 minutes, then incubated for 30 minutes in TBS-T/5% BSA/5% goat serum, followed by incubation with the following antibodies: rabbit anti-wide spectrum Cytokeratin (Abcam; 1:100), mouse-anti-human Vimentin (Abcam; 1:100), mouse-anti-human p53 (Santa Cruz; 1:100) overnight at 4°C. The following day, slides were washed 3 times in TBS and incubated with the appropriate secondary antibodies: goat-anti-rabbit-Alexa594 (Invitrogen; 1:1000) plus goat-anti-mouse-Alexa488 (Invitrogen; 1:400) for pan-CK and Vimentin; or goat-anti-mouse-Alexa594 (Invitrogen; 1:200) for p53. Secondaries were incubated for 1 hour at room temperature. Slides were then washed and incubated for 1 minute in TBS with 1 µg/ml Hoechst 333258, then coverslipped with Mowiol 4-88 (Sigma).

FFPE Tissue Sections

Paraffin blocks of HGSOC tissues from 5 patients were obtained from the UHN Biospecimen Sciences Program (UHN, Toronto, ON) in accordance with regulations for excess tissue use stipulated by the UHN research ethics board. 4 µm sections were transferred onto positively-charged slides. Sections were deparaffinised using xylene and ethanol. For antigen retrieval, slides were incubated in 0.01 M citrate buffer (pH 6.0) with 0.05% Tween in a glass vessel submerged in boiling water for 20 minutes. Sections were then permeabilized in TBS-T (containing 0.1% Tween for Cytokeratin, CD49e and FAP, and 0.3% Triton X-100 for TCF21) for 10 minutes. Sections were incubated for 2 hours in TBS-T/0.5% BSA/5% goat serum, followed by incubation with rabbit anti-human TCF21 (Sigma, 1:100), mouse-anti-human-CD49e (BD Biosciences, 1:100), mouse-anti-human-FAP (R&D Systems, 1:50), and either mouse-anti-pan-Cytokeratin (Abcam, 1:100), or rabbit anti-wide spectrum Cytokeratin (1:100) overnight at 4°C. The following day, slides were washed 3 times and incubated with goat-anti-rabbit-Alexa594 (Invitrogen; 1:1000) plus goat-anti-mouse-Alexa488 (Invitrogen; 1:400) for 1 hour at room temperature. Slides were then washed and incubated for 1 minute in TBS with 1 µg/ml Hoechst 333258, then coverslipped with Mowiol 4-88 (Sigma). Slides were scanned using a Zeiss Axio Slide Scanner and images were analyzed using HALO software (Indica Labs).

Microarrays

HGSOC single cell suspensions were stained for fluorescence activated cell sorting (FACS) as described above. Doublets and dead cells were excluded and $CD31^{-}CD45^{-}EpCAM^{-}$

$CD49e^+$ cells, $CD31^-CD45^-EpCAM^+CD133^-$ cells, and $CD31^-CD45^-EpCAM^+CD133^+$ cells were gated for sorting based on FMO controls. Post-sort purity checks for each sample confirmed >98% purity for each population. Twelve patient samples were sorted into tubes containing Iscove's Modified Dulbecco's Medium (IMDM) with 10% FBS. Sorted populations were washed with PBS and then RNA was extracted immediately using the RNeasy Plus Micro kit (Qiagen). RNA quality was verified using a Bioanalyzer 2100 (Agilent Technologies). All samples had an RNA integrity number (RIN) >8. 5 ng of RNA per sample were amplified using the Ovation pica WTA V2 kit (Nugen) as per the manufacturer's instructions. Amplified cDNA from each sample was labelled following Nugen Illumina solution application Note #2. 750 ng of amplified biotin-labelled cDNA generated from these samples were randomized and hybridized onto three Illumina Human HT-12 v4 BeadChips. BeadChips were incubated at 48 °C at rotation speed 5 for 15 hours for hybridization. The BeadChips were washed and stained as per Illumina protocol and scanned on the iScan (Illumina). Data files were quantified in GenomeStudio Version 2011.1 (Illumina) and passed sampled-dependent and independent QC metrics.

Probe intensities were normalized between arrays using quantile normalization and transformed using the logarithm of base 2. Differential expression between the different groups of samples – CD49e+ and EpCAM+, FH and FL – was estimated using limma 3.28.21. HGNC gene names were associated with probe identities using biomaRt 2.28.0. Two-color heatmaps were generated using the heatmap.2 function of the gplots R package 3.0.1 and pvclust 2.0.0 was used to cluster the CAF FH and FL samples with bootstrapping.

To carry out pathway analysis of CD49e+ and EpCAM+ cells, an expression score was created to rank all genes from top up-regulated to top down-regulated using the formula 'sign(logFC) * -log10(pvalue)'. Gene set enrichment analysis (GSEA – Broad Institute) was applied on this rank list using 1000 permutations. The gene-sets tested by GSEA were the Reactome database included in the MSig c2.cp.reactome.v6.1.symbols.gmt file. Results were visualized in Cytoscape 3.6.1 using EnrichmentMap 3.1, clustered and annotated using AutoAnnotate 1.2. Cluster labels were manually edited for clarity.

qRT-PCR

Quantitative reverse transcription PCR (qRT-PCR) was performed in triplicate using Power SYBR Green PCR Master Mix (Life Technologies). Samples were loaded into a BioRad CFX96 real-time PCR detection system following the manufacturer's protocols. Relative amounts

of mRNA were calculated by the ΔΔCt method and normalized to expression levels of *UBC.* The following primer sequences were used:
FAP, forward 5′-TGGCGATGAACAATATCCTAGA-3′, reverse 5′-ATCCGAACAACGGGATTCTT-3′; *Col11a1*, forward 5′-TTTTCCAGGATTCAAAGGTGA-3′, reverse 5′-TGGGCCAATTTGACCAAC-3′; *Sulf1*, forward 5′-ACCAGACAGCCTGTGAACAA-3′, reverse 5′-ATTCGAAGCTTGCCAGATGT-3′; *TCF21*, forward 5′-CGACAAATACGAGAACGGGTA−3′, reverse 5′-TCAGGTCACTCTCGGGTTTC−3′; *Colec11*, forward 5′-CCCCTGGTCCTAATGGAGA−3′, reverse 5′-TCAGCTGAGAGACCTGGTTGT−3′; *Dlk1*, forward 5′-GACGGGGAGCTCTGTGATAG−3′, reverse 5′-GGGCACAGGAGCATTCATA−3′; *UBC*, forward 5′-AGGCAAAGATCCAAGATAAGGA-3′, reverse 5′-GGACCAAGTGCAGAGTGGAC−3′.

RNA-Seq

HGSOC single cell suspensions were stained for FACS as described above. Doublets and dead cells were excluded and CD45-CD31-EpCAM-CD49e+FAP-High and CD45-CD31-EpCAM-CD49e+FAP-Low populations were gated for sorting. At least 10000 cells were sorted from each population. Twelve patient samples were sorted into tubes containing Iscove's Modified Dulbecco's Medium (IMDM) with 10% FBS. Sorted populations were washed with PBS and then RNA was extracted immediately using the RNeasy Plus Micro kit (Qiagen). RNA samples were assessed on a RNA 6000 Pico chip (Agilent Technologies) using the Agilent Bioanalyzer to determine sample RIN and quantified by the Qubit RNA HS assay kit (Life Technologies). All samples used had RIN values greater than 8.5. 4 ng of RNA were used to prepare RNA libraries using the SMARTer Stranded Total RNA-seq Kit – Pico Input Mammalian (Takara Bio USA Inc.). Briefly, the samples underwent first-strand synthesis *via* random priming oligos on the 3’ end. A template switching oligo mix (TSO) was then incorporated to allow the RT reaction to continue replicating the 5’ of the RNA strand. Following this, the samples were PCR amplified to incorporate full-length Illumina adapters and sample barcodes by binding to either the TSO stretch on the 5’ end, or the random priming oligo sequence on the 3’ end. The amplified cDNA is treated with ZapR which specifically targets ribosomal RNA in the presence of mammalian-specific R-Probes. This process leaves non-ribosomal RNA untouched, while ribosomal RNAs are cleaved, leaving them non-amplifiable. A final PCR reaction was done to enrich the uncut strands of cDNA

to generate the final RNA library. Final RNA library sizing was verified on the Agilent high sensitivity DNA kit (Agilent Technologies) using the Agilent Bioanalyzer while library concentration was quantified by qPCR using the KAPA SYBR FAST qPCR kit (Kapa Biosystems). Libraries were normalized to 10nM, diluted to 2nM, denatured using 0.2N NaOH, and diluted again to 1.7pM before loading onto the NextSeq 500 system. The samples were sequenced using a paired-end 75 cycle sequencing run to achieve a minimum of ~40M reads per sample.The reads were mapped using STAR/2.5.2 to the hg38 reference genome. Read counts per gene were obtained through htseq-count v.0.6.1. After removing low count genes whose cpm (counts per million reads) were less than 0.75 to in one third of the total number of samples, the edgeR R package v.3.8.6 was used to normalize the data using the TMM (trimmed mean of M values) method and to estimate differential expression by applying a generalized linear model between the FL fraction samples and the FH fraction samples. The multidimensional scaling plot was created using the edgeR plotMDS.DGEList() function.

For pathway analysis of FH and FL CAFs, an expression score was created to rank all genes from top up-regulated to top down-regulated using the formula sign(logFC) * -log10(pvalue). Gene set enrichment analysis (GSEA – Broad Institute) was applied on this rank list using 1000 permutations. The gene-sets tested by GSEA were first the microarray FH and FL gene lists and second gene-sets from the Reactome database included in the MSig c2.cp.reactome.v6.1.symbols.gmt file. Results were visualized in Cytoscape 3.6.1 using EnrichmentMap 3.1, clustered and annotated using AutoAnnotate 1.2. Cluster labels were manually edited for clarity.

TCGA Data Analysis

To identify genes specific to FH and FL CAFs, genes differentially expressed between FH and FL fractions at a FDR cut-off of 0.05 and with a logFC greater than 2 fold (logFC >2 for FH and <-2 for FL) were selected. These genes were then filtered to include only those that have a higher expression in CD49e+ cells compared to EpCAM+ CD133+ at a FDR cut-off of 0.05 in the Human Illumina HT-12 V4 array. This generated a list of 165 FH CAF-specific genes and 78 FL-specific genes.

HGSOC data were downloaded from the Genomic Data Commons (GDC) Data Portal (https://portal.gdc.cancer.gov/). HiSeq gene level counts (level2 RNA-Seq data) and corresponding clinical data were downloaded for 374 samples included in this analysis.

Trimmed mean of M values (TMM) followed by count per million (CPM) and logarithm of base 2 transformation was used to normalize the data within the edgeR package. Data were selected to only contain the FH and FL gene list and a heatmap was created using R heatmap.2. Color bars were added to the heatmap to identify patients based on molecular phenotype described by (Verhaak et al., 2013). These phenotypes include the categories 'mesenchymal', 'immune', 'proliferative', and 'differentiated' and they were extracted from Supplemental Table 1 of (Verhaak et al., 2013). Differential expression was calculated within edgeR for samples defined as 'mesenchymal' versus all the other samples and a list ranking genes from top up-regulated to down regulated was generated using the formula 'sign(logGC) * -log10(pvalue)'.

FH and FL color bar: TCGA patients were ranked using a score that counts how many genes from the FH gene list or FL gene list have a normalized value greater than the patient mean (i.e. a z-score). Patients were considered FH if they had positive scores for at least 75% of the gene list (corresponding to a sum of z-scores > gene list length/2). A less tringent threshold classified patients as FH or FL if they had positive scores in at least 50% of the gene list (corresponding to a sum of z-scores > 0). The FH and FL patient categories were added to the heatmap color bar and used for further analysis.

TCGA patients were then grouped into 'FH' and 'FL' and 'other' categories using either the 75% or the 50% thresholds and ESTIMATE and ABSOLUTE values, which are known to measure percentage of stromal cell and tumor purity content, respectively (Carter et al., 2012; Yoshihara et al., 2013) were determined using the respective R packages. Data were plotted on a whisker boxplot for each category. Clinical data including overall survival and progression free events were retrieved for TCGA patients falling into the FH and FL categories based on the more stringent 75% cut-off and Kaplan-Meier curves were generated and associated with a log rank test using GraphPad Prism software.

For GSEA testing of the short FH and FL lists in the 'mesenchymal' subtype, the mesenchymal rank list was tested against the short FH and FL gene lists using default parameters.

Proliferation Assays

FH and FL CAFs were isolated from primary HGSOC patient samples using FACS, as described above. 5000 cells/well from each subset were seeded in triplicate into 96-well plates in IMDM with 10% FBS. Growth of cells was monitored for a period of 10-14 days. Cell confluence was measured and quantified by the IncuCyte ZOOM live cell imaging system (Essen Biosciences).

Gel Contraction

FH and FL CAFs were suspended in IMDM with 10% FBS at a concentration of 100,000 cells/ml and kept on ice. 3 mg/ml Collagen-I solution (Thermo-Fisher Corning, 354236) and 1M NaOH were then added to the cell suspension give a final concentration of 1mg/ml Collagen-I and a neutral pH, and 100 µl were aliquotted into non-tissue culture-treated flat-bottom 96-well plates. Plates were left for 20 minutes at room temperature to solidify, then 120 µl IMDM + 10% FBS was added to the wells. A small pipet tip was gently run around the perimeter of each well prior to imaging on the Incucyte ZOOM every 6 hours for 3 days. The areas of the gels at different time points were quantified using ImageJ (Fiji) software.

3D Spheroid Invasion Assays

GFP-expressing HGSOC cell lines (OVCAR8, OV90 and ES2) were mixed with either FH, FL, 851FH-TCF21, or 851FH-GFP CAFs at a ratio of 5:1 (CAF: cancer cells). 6000 total cells per well were then plated in 90 µl basal media (IMDM for OVCAR8, McCoy's 5A for ES2, or MCDB105: M199 for OV90) supplemented with 2% FBS in ultra-low attachment round bottom 96 well plates (Corning, 7007). Plates were centrifuged at low speed to center the cell suspension prior to incubation at 37°C for 3 days. At that point, spheroids were formed and 30 µl of media were removed from each well and replaced with 30 µl of growth factor reduced Matrigel (Corning, 354230) to give a final Matrigel concentration of 33% v/v. Plates were incubated for 60 minutes at 37°C, then 100 µl per well of the appropriate basal media supplemented with 2% FBS was added and plates were returned to the incubator. The time point used to quantify invasion was optimized for individual cell lines, and ranged from 1 day (for ES2 cells) to 4 days (for OVCAR8 and OV90 cells). Spheroids were imaged with a Zeiss LSM700 confocal microscope. Circularity of spheroids (OVCAR 8, OV90) and cell counts outside the spheroid (ES2) were analyzed using ImageJ (Fiji) software. In some cases, multiple spheroids formed per well, or the spheroids were not centered in

the well and thus could not be imaged. However, a minimum of 5 and up to 10 spheroids per experimental group were analyzed in all cases.

In Vitro Carboplatin Treatment

1000 cells per well of GFP or mCherry-expressing OVCAR8, OV90 or ES2 cells were seeded in their respective media onto a monolayer of CAFs in 96-well flat-bottom tissue culture plates. The plates were incubated at 37°C for 24 hours, then carboplatin (Hospira) was added to reach a final concentration of 10 μM. Cancer cell proliferation was monitored using Incucyte ZOOM live cell imaging system for up to 10 days.

In Vivo Assays

HGSOC OVCAR8 cells constitutively expressing firefly luciferase were mixed with FH, FL, 851FH-TCF21 or 851FH-GFP CAFs at a ratio of 5:1 (CAF: cancer cells). OVCAR8 cells alone were used as a control. Spheroids were formed as described above and suspended in a final volume of 100 μl IMDM media supplemented with 2% FBS. 100 μl of growth factor reduced Matrigel was added to the wells, mixed gently, then immediately loaded into blunt-end 16 gauge syringes (Stemcell Technologies, 28110). 6-8 week old female NSG mice were anaesthetized with isoflurane and an incision was made near the fourth mammary fat pad. Spheroids were then implanted into the fat pad directly and the incision was stapled. Mice were injected weekly with 30 mg/ml luciferin (Cedarlane) and imaged using a Xenogen IVIS Imaging System 100. Signal was quantified using IVIS Living Image software.

Lentiviral Constructs

Custom lentiviral vectors were designed and plasmids obtained using VectorBuilder (Cyagen Biosciences). A PGK promoter-driven *TCF21*-P2A-GFP lentiviral vector and control PGK-GFP and PGK-mCherry vectors were designed and purchased from Vectorbuilder (Cyagen Biosciences). For lentiviral infections cells were plated in 6-well plates at 1.0×10^5 cells per well and incubated with viral supernatants for 48 hours at 37°C. Infected cells were purified by FACS on the basis of GFP or mCherry expression and expanded for further use.

TCF21 Western Blot

851FH-GFP and 851FH-TCF21 CAFs were lysed in RIPA lysis buffer supplemented with EDTA-free protease inhibitor cocktail tablets (Roche) and normalized for total protein amount. 35

μg of protein from each sample were resolved in a 12% SDS-PAGE gel, and transferred onto Immobilon-P membranes (Millipore) using a semi-dry transfer method (Bio-Rad). Blots were probed overnight at 4°C using a mouse-anti-human ERK2 antibody (Santa Cruz; 1:1000) and a rabbit-anti-human TCF21 antibody (Sigma; 1:250), followed by a 45-minute incubation at room temperature with a goat anti-mouse IgG HRP-linked secondary antibody (Invitrogen, 1:1000), and goat-anti-rabbit IgG HRP-linked secondary antibody (Cell Signaling, 1:2500). Proteins were detected using enhanced chemiluminescence reagent (ThermoFisher) and autoradiograph exposure (Sigma-Aldrich).

Quantification and Statistical Analysis

Information about statistical details and analysis of microarray and RNAseq data is indicated in text, figure legends, or method details. Graphs and statistical values (p-values, correlation coefficients, hazard ratios) were generated using Graphpad Prism 6.03. Error bars indicate standard error of the mean (SEM) or standard deviation (SD) for a minimum of three independent experiments.

SUPPLEMENTAL INFORMATION

Table S1 – Clinical Information and %FAP+ CAFs in Primary Tumor Specimens Used in This Study

Table S2A - Differentially Expressed Genes Between FACS Isolated CD49e+ CAFs and EpCAM+CD133+ Epithelial Cells

Table S2B - Differentially Expressed Gene Sets (MsigDB Reactome) Between FACS Isolated CD49e+ CAFs and EpCAM+CD133+ Epithelial Cells

Table S3A - Differentially Expressed Genes Between FH and FL Clusters of Isolated CD49e+ CAFs

Table S3B – Differentially Expressed Genes Between FL CAFs and Normal Stroma in the Leung et al Dataset.

Table S4A – Differentially Expressed Genes Between FACS-Purified FH and FL CAFs

Table S4B - Differentially Expressed Gene Sets (MsigDB REactome + GO BP and MF) Between FACS-Purified FH and FL CAFs

Table S5 – Gene Signature Used to Interrogate TCGA Data

Figure S1. Identification of CD49e as a CAF-specific cell surface marker

Figure S2. Isolation and transcriptional profiling of CD49e+ CAFs

Figure S3. IF staining and quantification of FAP and TCF21 in HGSOC specimens

FigureS4. FH and FL gene lists and FH/FL TCGA patient classification

Figure S5. Schematics for *in vitro* and *in vivo* spheroid assays

Figure S6. Chemotherapy treatment of HGSOC cell lines

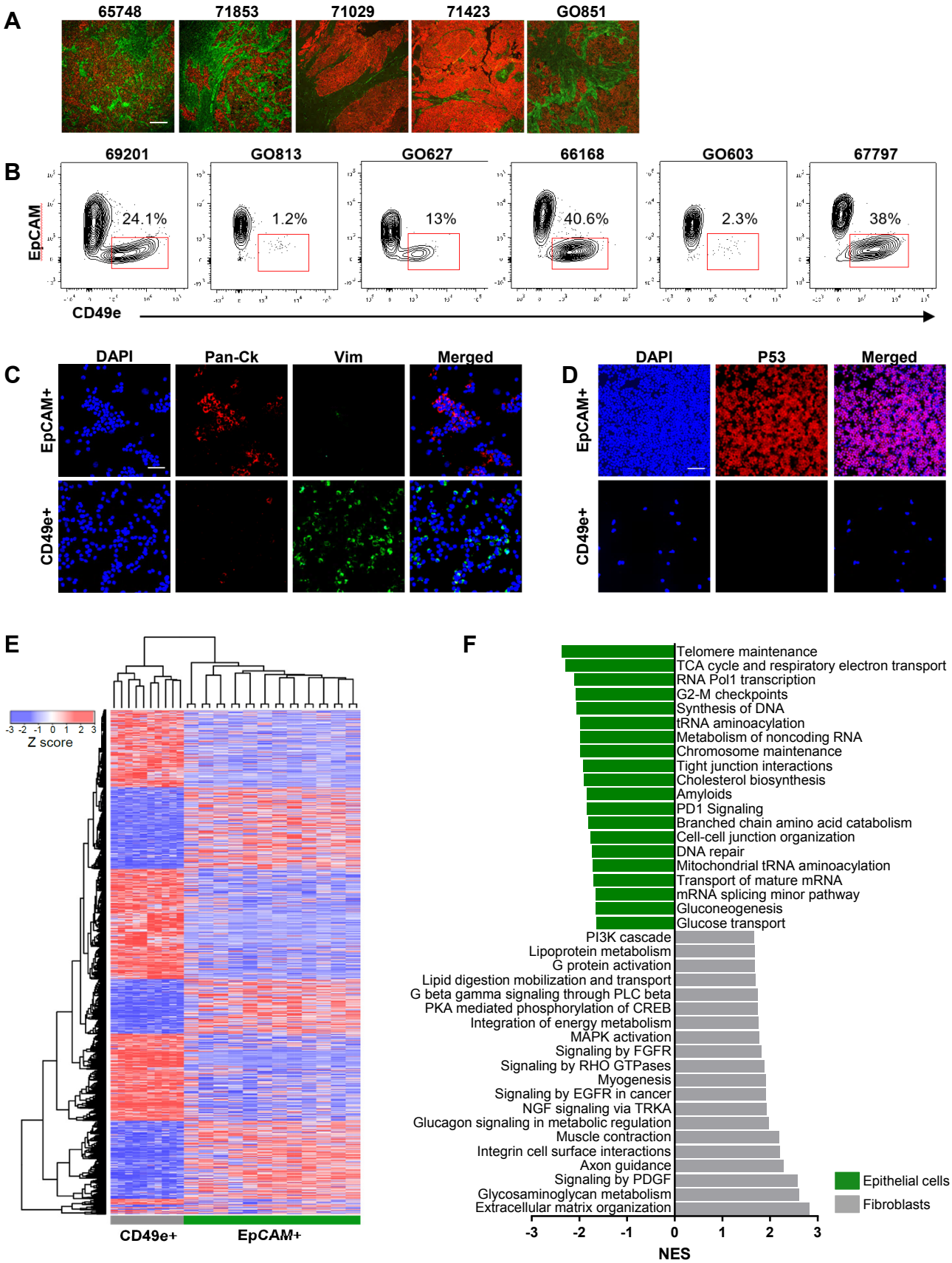
A
65748
71853
71029
71423
GO851
B
69201
GO813
GO627
66168
GO603
67797
24.1%
1.2%
13%
40.6%
2.3%
38%
EpCAM
CD49e
C
DAPI
Pan-Ck
Vim
Merged
EpCAM+
CD49e+
D
DAPI
P53
Merged
EpCAM+
CD49e+
E
-3 -2 -1 0 1 2 3
Z score
CD49e+
EpCAM+
F
Telomere maintenance
TCA cycle and respiratory electron transport
RNA Pol1 transcription
G2-M checkpoints
Synthesis of DNA
tRNA aminoacylation
Metabolism of noncoding RNA
Chromosome maintenance
Tight junction interactions
Cholesterol biosynthesis
Amyloids
PD1 Signaling
Branched chain amino acid catabolism
Cell-cell junction organization
DNA repair
Mitochondrial tRNA aminoacylation
Transport of mature mRNA
mRNA splicing minor pathway
Gluconeogenesis
Glucose transport
PI3K cascade
Lipoprotein metabolism
G protein activation
Lipid digestion mobilization and transport
G beta gamma signaling through PLC beta
PKA mediated phosphorylation of CREB
Integration of energy metabolism
MAPK activation
Signaling by FGFR
Signaling by RHO GTPases
Myogenesis
Signaling by EGFR in cancer
NGF signaling via TRKA
Glucagon signaling in metabolic regulation
Muscle contraction
Integrin cell surface interactions
Axon guidance
Signaling by PDGF
Glycosaminoglycan metabolism
Extracellular matrix organization
-3 -2 -1 0 1 2 3
NES
Epithelial cells
Fibroblasts

Figure 1

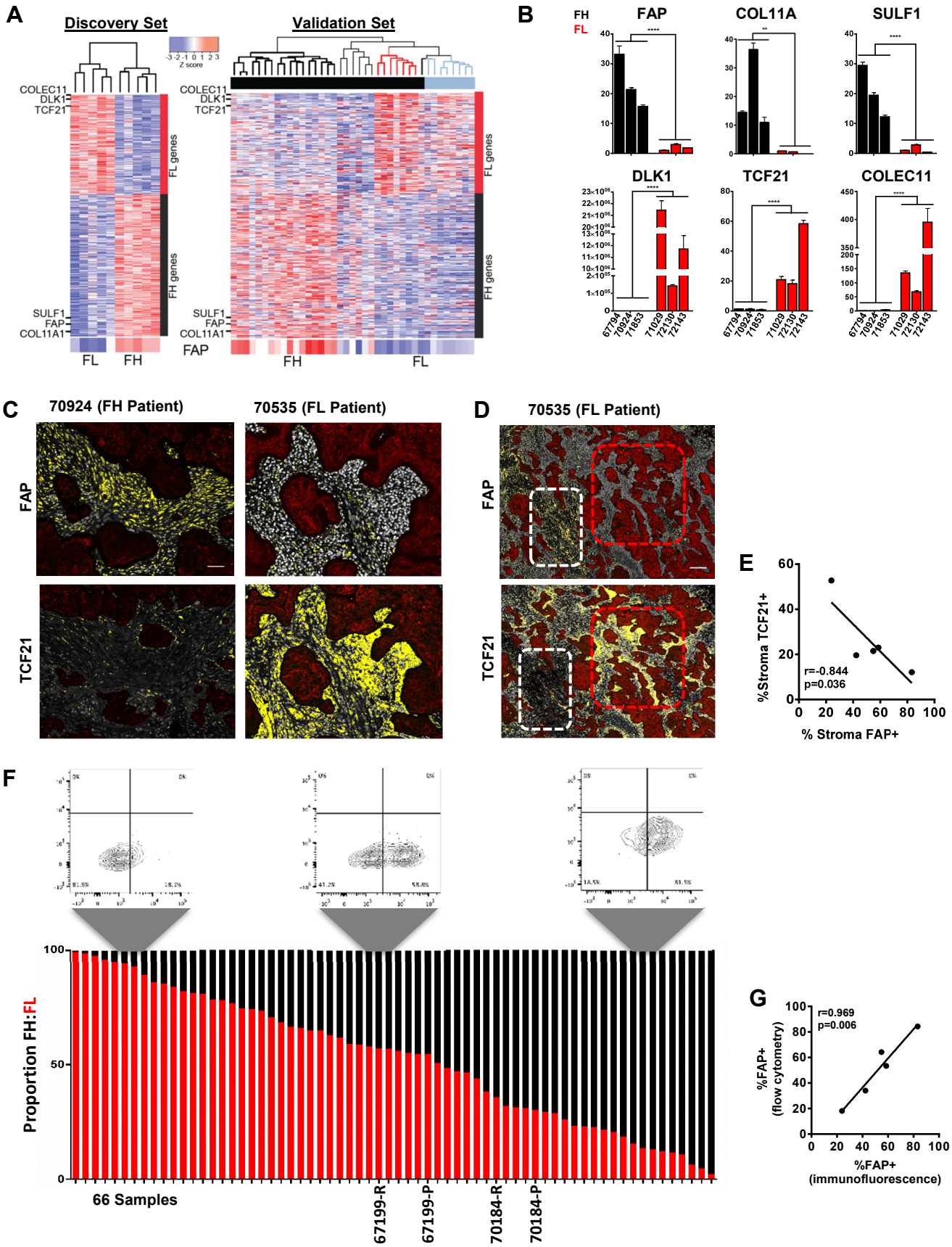
A
Discovery Set
Validation Set
Z score
COLEC11
DLK1
TCF21
SULF1
FAP
COL11A1
FL genes
FH genes
FL
FH
B
FH
FL
FAP
COL11A
SULF1
DLK1
TCF21
COLEC11
67794
70924
71853
71029
72130
72143
C
70924 (FH Patient)
70535 (FL Patient)
FAP
TCF21
D
70535 (FL Patient)
E
%Stroma TCF21+
% Stroma FAP+
r=-0.844
p=0.036
F
Proportion FH:FL
66 Samples
67199-R
67199-P
70184-R
70184-P
G
%FAP+ (flow cytometry)
%FAP+ (immunofluorescence)
r=0.969
p=0.006

Figure 2

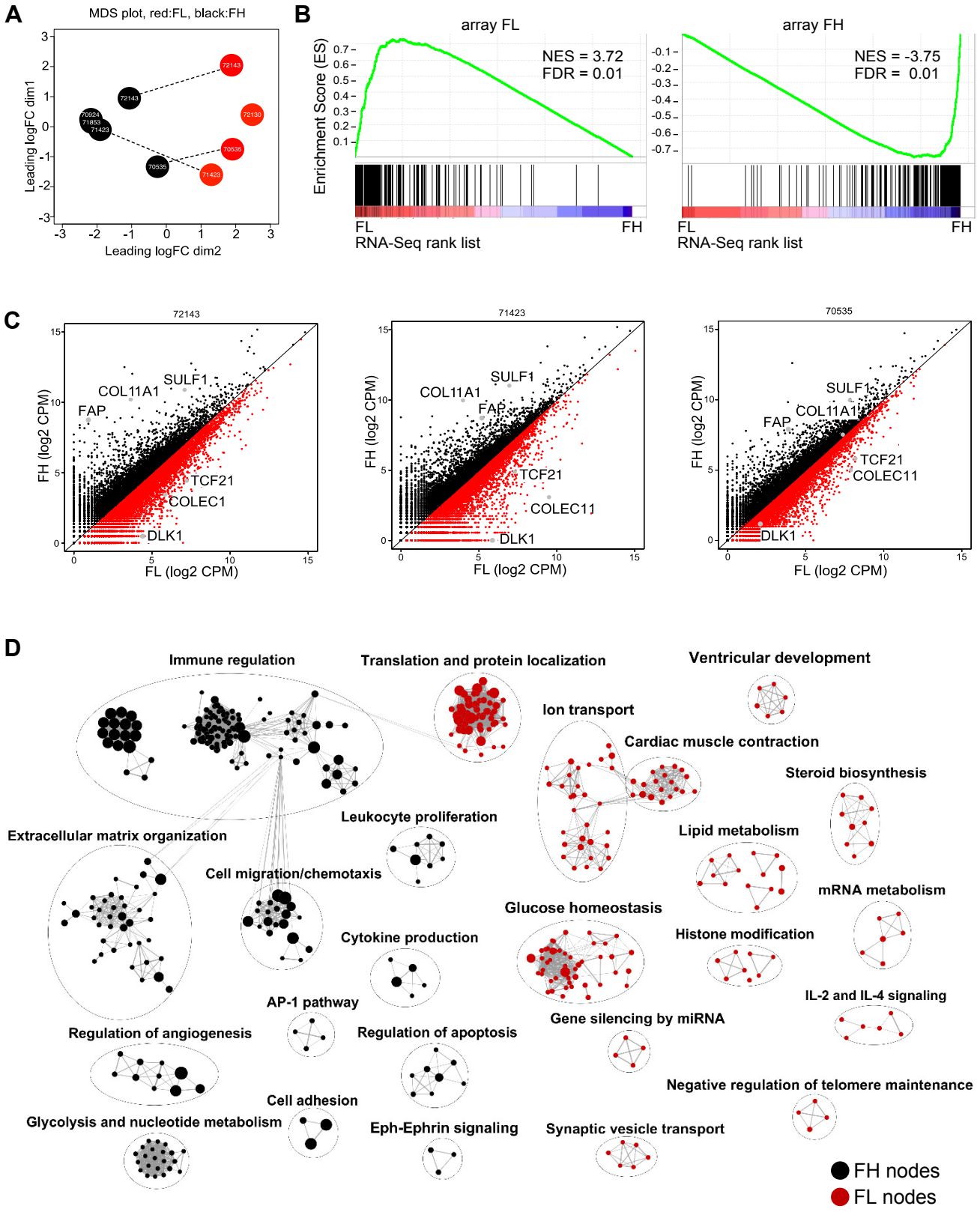
A
MDS plot, red:FL, black:FH
Leading logFC dim1
Leading logFC dim2
B
array FL
NES = 3.72
FDR = 0.01
Enrichment Score (ES)
FL
FH
RNA-Seq rank list
array FH
NES = -3.75
FDR = 0.01
FL
FH
RNA-Seq rank list
C
72143
71423
70535
FH (log2 CPM)
FL (log2 CPM)
SULF1
COL11A1
FAP
TCF21
COLEC1
COLEC11
DLK1
D
Immune regulation
Translation and protein localization
Ventricular development
Ion transport
Cardiac muscle contraction
Steroid biosynthesis
Leukocyte proliferation
Extracellular matrix organization
Lipid metabolism
Cell migration/chemotaxis
mRNA metabolism
Glucose homeostasis
Cytokine production
Histone modification
AP-1 pathway
IL-2 and IL-4 signaling
Gene silencing by miRNA
Regulation of angiogenesis
Regulation of apoptosis
Negative regulation of telomere maintenance
Cell adhesion
Glycolysis and nucleotide metabolism
Eph-Ephrin signaling
Synaptic vesicle transport
FH nodes
FL nodes

Figure 3

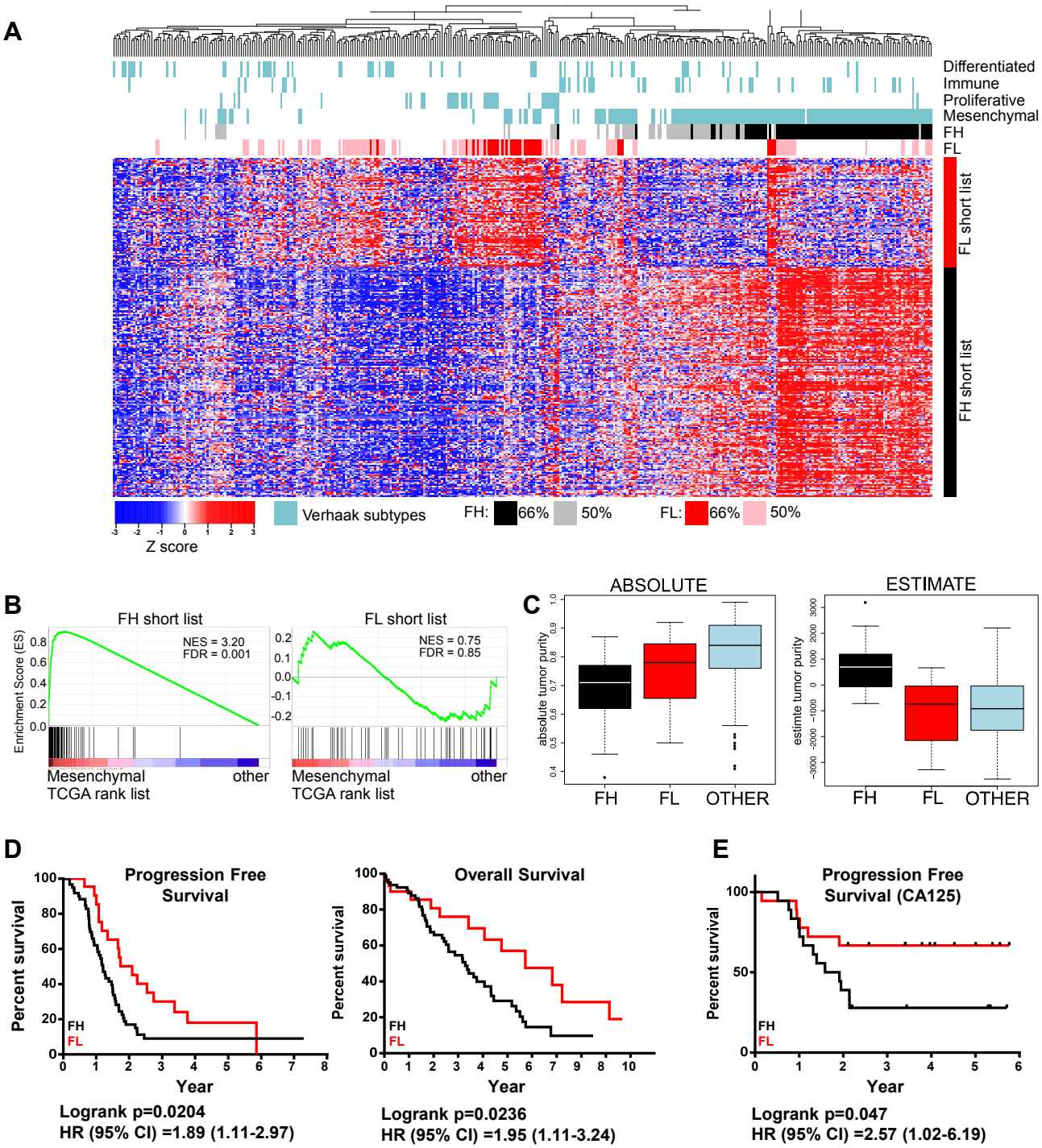
A
Differentiated
Immune
Proliferative
Mesenchymal
FH
FL
FL short list
FH short list
Z score
Verhaak subtypes
FH: 66% 50%
FL: 66% 50%
B
FH short list
NES = 3.20
FDR = 0.001
Enrichment Score (ES)
Mesenchymal
other
TCGA rank list
FL short list
NES = 0.75
FDR = 0.85
Mesenchymal
other
TCGA rank list
C
ABSOLUTE
absolute tumor purity
FH
FL
OTHER
ESTIMATE
estimte tumor purity
FH
FL
OTHER
D
Progression Free Survival
Percent survival
Year
FH
FL
Logrank p=0.0204
HR (95% CI) =1.89 (1.11-2.97)
Overall Survival
Percent survival
Year
FH
FL
Logrank p=0.0236
HR (95% CI) =1.95 (1.11-3.24)
E
Progression Free Survival (CA125)
Percent survival
Year
FH
FL
Logrank p=0.047
HR (95% CI) =2.57 (1.02-6.19)

Figure 4

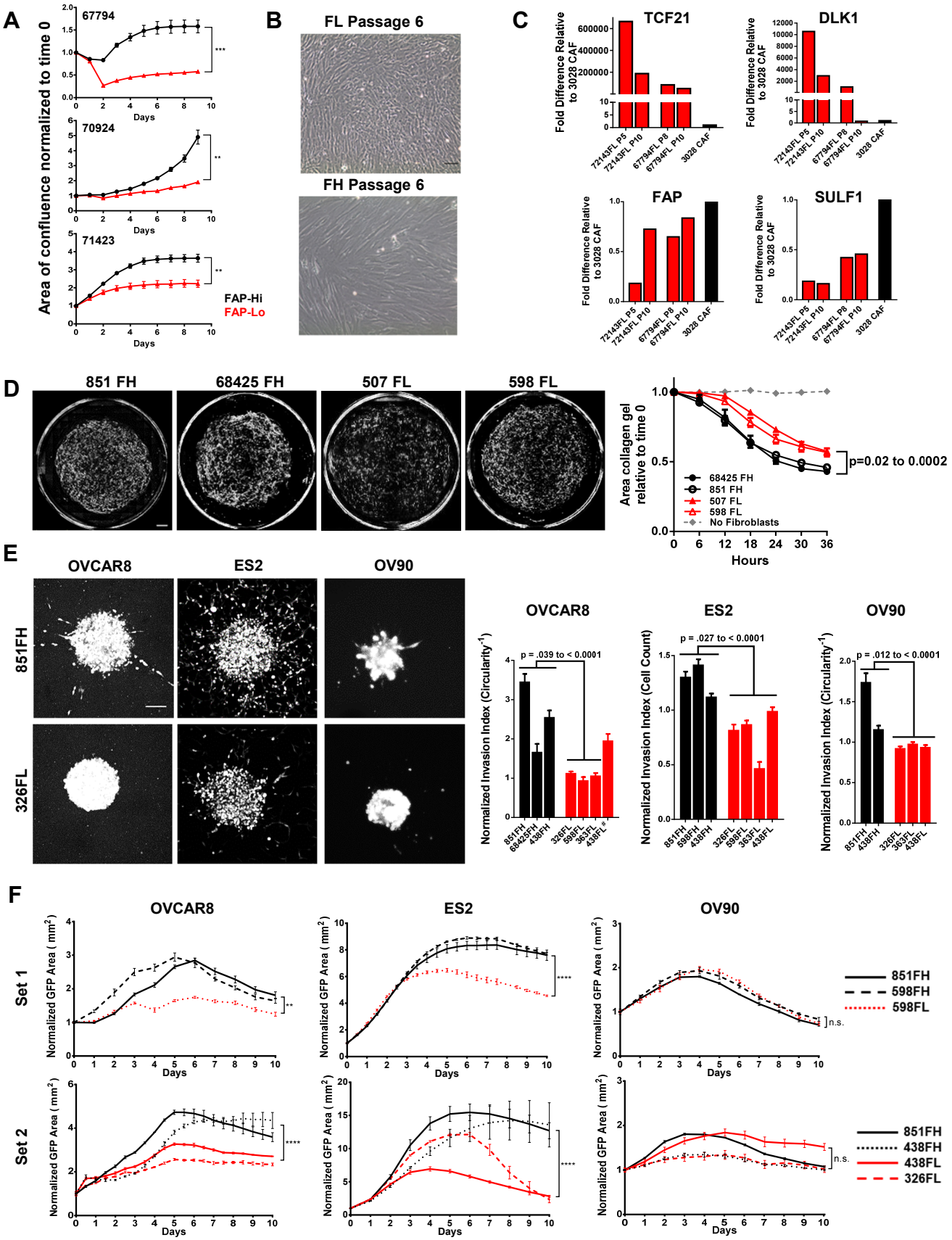
A
67794
70924
71423
Area of confluence normalized to time 0
Days
FAP-Hi
FAP-Lo
B
FL Passage 6
FH Passage 6
C
TCF21
DLK1
FAP
SULF1
Fold Difference Relative to 3028 CAF
72143FL P5
72143FL P10
67794FL P8
67794FL P10
3028 CAF
D
851 FH
68425 FH
507 FL
598 FL
Area collagen gel relative to time 0
Hours
68425 FH
851 FH
507 FL
598 FL
No Fibroblasts
p=0.02 to 0.0002
E
OVCAR8
ES2
OV90
851FH
326FL
Normalized Invasion Index (Circularity-1)
Normalized Invasion Index (Cell Count)
p = .039 to < 0.0001
p = .027 to < 0.0001
p = .012 to < 0.0001
F
Set 1
Set 2
Normalized GFP Area (mm2)
Days
851FH
598FH
598FL
438FH
438FL
326FL
n.s.

Figure 5

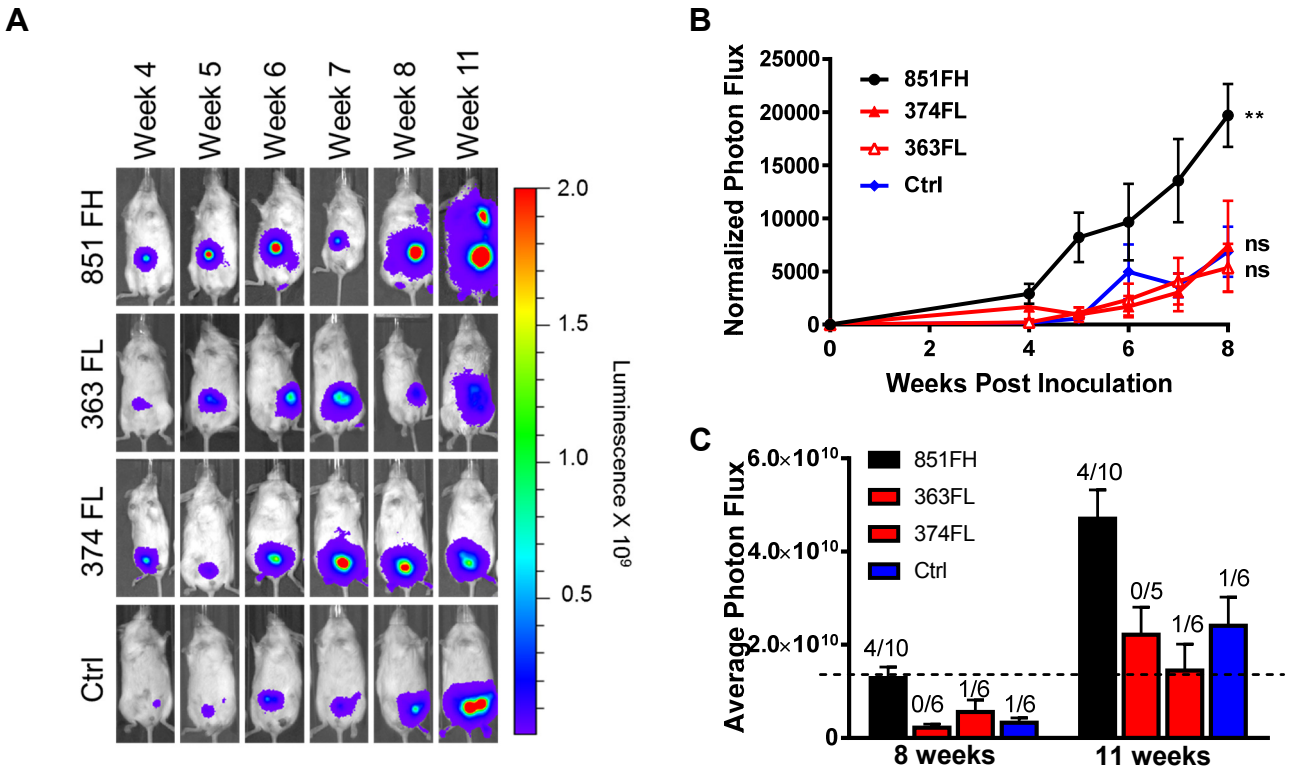
A
Week 4
Week 5
Week 6
Week 7
Week 8
Week 11
851 FH
363 FL
374 FL
Ctrl
2.0
1.5
1.0
0.5
Luminescence X 10⁹
B
Normalized Photon Flux
25000
20000
15000
10000
5000
0
851FH
374FL
363FL
Ctrl
**
ns
ns
0
2
4
6
8
Weeks Post Inoculation
C
Average Photon Flux
6.0×10¹⁰
4.0×10¹⁰
2.0×10¹⁰
0
851FH
363FL
374FL
Ctrl
4/10
0/6
1/6
1/6
4/10
0/5
1/6
1/6
8 weeks
11 weeks

Figure 6

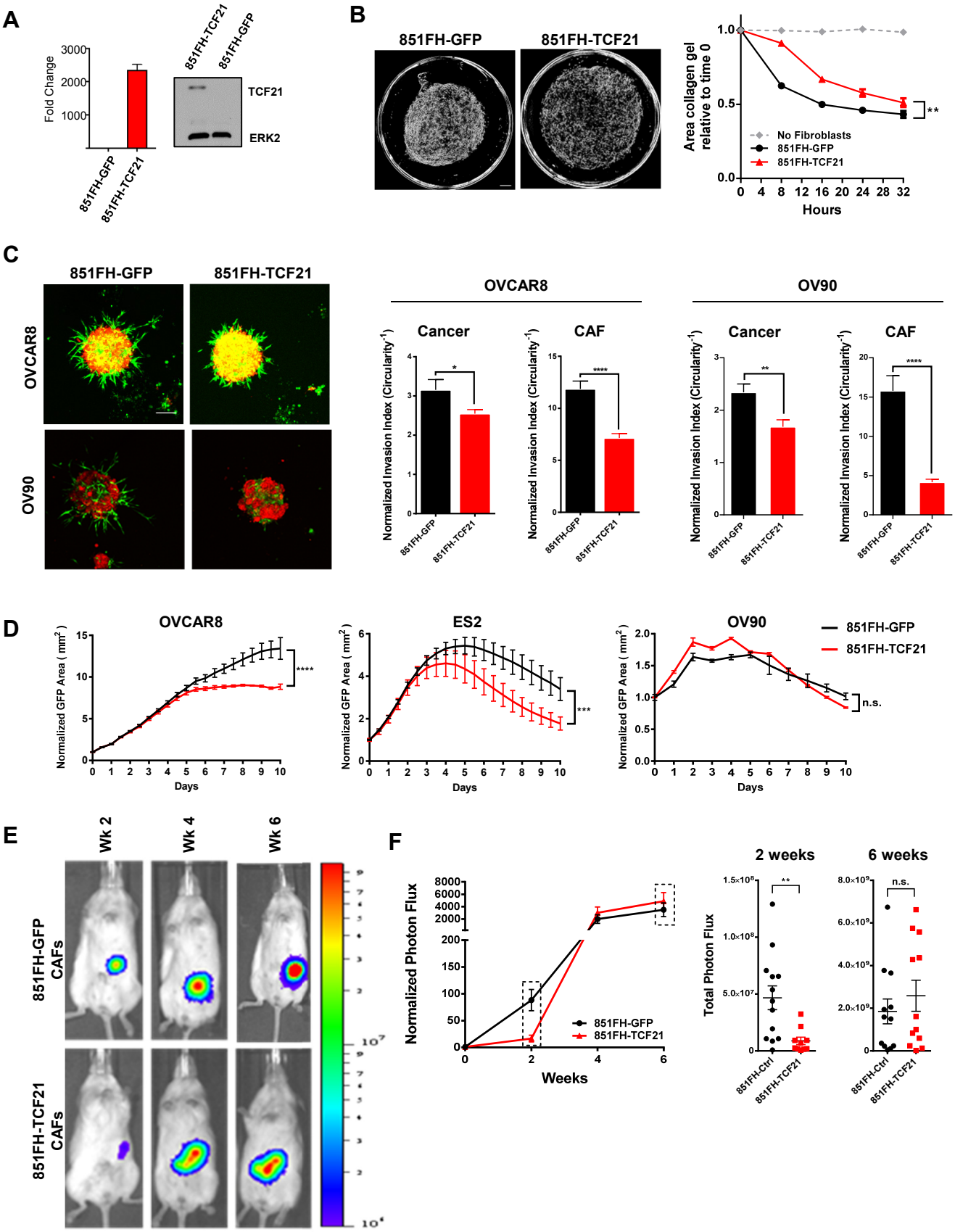
A
Fold Change
3000
2000
1000
851FH-GFP
851FH-TCF21
851FH-TCF21
851FH-GFP
TCF21
ERK2
B
851FH-GFP
851FH-TCF21
Area collagen gel relative to time 0
1.0
0.5
0.0
**
No Fibroblasts
851FH-GFP
851FH-TCF21
0 4 8 12 16 20 24 28 32
Hours
C
851FH-GFP
851FH-TCF21
OVCAR8
OV90
OVCAR8
OV90
Cancer
CAF
Cancer
CAF
Normalized Invasion Index (Circularity-1)
*
****
**
****
851FH-GFP
851FH-TCF21
D
OVCAR8
ES2
OV90
Normalized GFP Area (mm2)
****
***
n.s.
Days
851FH-GFP
851FH-TCF21
E
Wk 2
Wk 4
Wk 6
851FH-GFP CAFs
851FH-TCF21 CAFs
F
Normalized Photon Flux
8000
6000
4000
2000
200
150
100
50
0
0 2 4 6
Weeks
851FH-GFP
851FH-TCF21
2 weeks
6 weeks
Total Photon Flux
1.5×10^8
1.0×10^8
5.0×10^7
0
**
8.0×10^9
6.0×10^9
4.0×10^9
2.0×10^9
0
n.s.
851FH-Ctrl
851FH-TCF21

Figure 7